Progress in Fractional Differentiation and Applications
An International Journal

http://dx.doi.org/10.18576/pfda/120205

Investigation of Buruli Ulcer and Cholera Mathematical Model Through Fractional Order Derivative Using Deep Neural Network

Mohammed A. El-Shorbagy [1], *Adnan Sami*[2], *Mati ur Rahman*[3,*] *and Hossam A. Nabwey*[1]

[1] Department of Mathematics, College of Science and Humanities in Al-Kharj, Prince Sattam bin Abdulaziz University, Al-Kharj 11942, Saudi Arabia
[2] Department of Mathematics, University of Malakand, Dir(L), Khyber Pakhtunkhwa, Pakistan
[3] Department of Mathematics and Statistics, College of Sciences, Imam Mohammad Ibn Saud Islamic University (IMSIU), Riyadh, Saudi Arabia

Received: 5 Jan. 2026, Revised: 8 Feb. 2026, Accepted: 22 Mar. 2026
Published online: 1 Apr. 2026

Abstract: Here, we present a comprehensive investigation of a complex epidemiological model incorporating power-law, exponential, and Mittag–Leffler kernels governed by the fractal–fractional Caputo (FFC) derivative. The model describes the dynamics of disease transmission and progression through multiple interacting compartments, including susceptible humans S_h, infected and recovered subgroups $I_b, I_c, R_b, R_c, R_{bc}$, and the interaction with environmental or vector-based reservoirs B and secondary susceptible/infected populations S_v, I_v. The FFC operator ${}^{\mathrm{FFC}}\mathrm{D}^{\tau,\kappa}$ is employed in each governing equation to capture the memory and hereditary effects inherent in biological systems. Key epidemiological processes, such as primary and secondary infections, cross-infection rates, recovery, and reinfection mechanisms, are explicitly incorporated. Both analytical and numerical techniques are utilized to examine the qualitative behavior and stability of the solutions within the FFC framework. A semi-analytical solution for the Buruli ulcer and cholera model is obtained using the Adams–Bashforth method. Numerical simulations are performed in MATLAB for both integer and non-integer orders within the interval (0,1). The simulation results demonstrate solution stability and single-point convergence, with a significant enhancement in stability observed for lower non-integer orders. Furthermore, the simulations are extended using a deep neural network approach for the considered model. Two hidden layers are employed, using hyperbolic tangent and linear activation functions, respectively. The dataset is divided into training, testing, and validation phases. Overall, the findings highlight the effectiveness and adaptability of fractal–fractional calculus in modeling complex temporal dynamics and provide deeper insights into disease management strategies in memory-dependent epidemiological environments.

Keywords: Epidemic diseases; Cholera Buruli Ulcer; Fractional derivative; Qualitative Analysis; Stability; Numerical Analysis; Deep Neural Network.

1 Introduction

The goal of mathematical modeling is to develope for epidemic disease to investigate the nonlinear process contains harmful diseases dynamics and identify the most effective strategy for managing them [1,2,3,4,5]. Ordinary and partial differential equations are frequently used to build mathematical models, and fractional differential equations, which generalize these models, are now thought to be highly effective. Realize that these models are taken into consideration and are thought to be very successful. As an illustration, consider the fractional derivative modeling of Hepatitis E disease [1], utilizing two variables in real-world problem for modeling [2], the recently defined nonintegers order derivative for epidemic models [3], applications of piece wise differential equations are in [4], and the corona virus (COVID-19) model [5]. Moreover, generally for better understanding and to the best of knowledge first the models formulated in ordinary differential equations form and then generalized to fractional oerders model.
Illnesses known as infectious disorders lived-in when microbes enters to body and proliferate. Samples of microorganisms that diverse life forms cause diseases include bacteria, viruses, archaea, and algae. Among other

* Corresponding author e-mail: mrmahman@imamu.edu.sa

infectious disorders, the Mycobacterium ulcerans is the microorganism of Buruli ulcer (BU), also called necrotizing skin disease [6]. Currently, this diseas has been identified in various region all over the world, where the tropical regions has a big ratio. The tropical region contains a number of nations with high infection rates. The majority of West African nation, notably Ghana, Cote dÍvoire, Benin, and Cameroon, are the most common locations, accounting for almost 80% of all cases reported worldwide [7]. The disease is frequently found in centers in each endemic nation, which regrettably impacts the inhabitants of such areas, which are typically extremely disadvantaged and face significant obstacles in obtaining high-quality health-care in their local communities [8].

Early disease detection and the management of antibiotics, such as streptomycin and rifampicin, for atleast eight weeks are the only effective means of halting the spread of BU infection. In many severe cases, the lesion may require proper treatment or, more frequently, grafting which may speed up the healing process and ultimately help avoid abnormalities [9,10,11]. Hospitalized peoples are a hallmark of BU, which financially burdens both the state and those who are continue their treatment [12]. The first comprehensive surveillance system implemented nationwide in Ghana, discovered about 1200 cases of BU since from 1993 to 1998. Interestingly, over 9,000 cases were reported nationwide since from 2014 to 2004 [13]. The Ashanti region of Ghana, contains the most endemic district, Amansie West, which is closely linked to galamsey. Cholera outbreaks are frequently caused by unplugged pit holes in these communities. An environment that is friendly for the extension of Mycobacterium ulcerans is produced by illicit mining activities. This later exposes children to arsenic in the environment and impairs their immune systems, which are still developing [14]. As a result, they are more vulnerable to a many kinds of illnesses, very commonly cholera, which is brought on by insufficient sanitations brought on by the extreme poverty in the communities. In 19th century, Cholera was identified by Jhon Snow. Guinea, a country in West Africa, is thought to have been the first to announce about cholera, a disease that is highly prevalent in Sub-Saharan Africa and Togolese patients was diagnosed with cholera at Kotoka International Airport on the first day of September 1970, marking the first known instance of the disease [15,16]. Ghana has experienced five significant cholera cases, the worst of which claimed 243 lives in 2014. According to estimates, the disease affects between 3 and 5 million individuals annually, with Asian and African nations accounting for the majority of cases [17]. Acute diarrhea brought on by intestinal infection with the Vibrio cholera bacteria is linked to this cholera infection. About 1 in 20 infected individuals show severe illness, and the infection maybe classified as asymptomatic, mild, or severe [18]. Watery diarrhea and vomiting are the hallmarks of cholera, and those who have it also lose water and become dehydrated. Individual lives are at stake and the effects are devastating when the intended treatment is not administered. Two methods of cholera transmission have been reported: aquatic reservoirs in the environment and diseased people themselves [19]. The quantity of infection can be decreased by decreasing the polluted surroundings. Generally, to stop the spread of cholera in the long run, every community needs to have good sanitation and good hygiene practices. In Sub-Saharan Africa, the two illnesses are highly prevalent, especially in Ghana, where artisans mining has resulted in a large number of stagnant water bodies and unsanitary circumstances that cause cholera. In these mining towns, stagnant water sources are typically home to Mycobacterium ulcerans [14]. A very important steps for developing the nations in West Africa, especially Ghana, to have a solid understanding of the two illnesses.

Studies on the mathematical models of Buruli ulcer and cholera have previously been supervised. Various investigations that are written in the form of mathematical models are present in the literature an effort to get focus on the nature of complexity of cholera dynamics. One of these was a mathematical model that the authors created that incorporated the echological dynamics of cholera into a standard SIR epidemiological equation [20]. By adding the pathogen's hyper-infectious characteristics, the authors of expanded the model from [20] and conducted an analysis. The authors in [21] further adjusted the dynamics of pathogen density infection in [12], paying special attention to in-reservoir pathogen dynamics and human environment interface.

In order to investigate intrprsonal transmission and surrounding to human transmission pathways, authors in [22] recently suggested a cholera model. The results of their study attempted to link interpersonal in a landlocked East African nation like Zimbabwe. Furthermore, without accounting for the saturation effect, the authors created a cholera model and included a dual transmission channel with bilinear incidence rates on both person-to-person and surrounding-to-person infection paths. In [23,24] the authors add some control terms and dual-infection dynamics of cholera's and malaria by comprising many times optimal overcome to manage the best plane to decline the combine infection of the diseases. Several mathematical models have been developed to study the epidemiology of BU. For instance, using a SIR structure model, the scientists in [14] came to the conclusion that water bug bites and arsenic surroundings both contribute to the spread of BU. The scientists put up an equation that aimed to represent the dynamics of BU transmission through two pathways: straight environmental contact with Mycobacterium ulcerans and water bug bites, which act as MU reservoirs [25]. Additionally, the authors in [26] developed a model and particularly examined the effects of BU in Ghana, coming to the conclusion that if present predictions are not altered, the dynamics stays unchanged. There are many combined infection mathematical models that formulated for other infectious disease, while

the proposed model (1) is the first to investigate on the co-infections of BU and cholera to the best of our knowledge.

A strong mathematical foundation for simulating intricate dynamical systems with memory, nonlocality, and inherited characteristics is fractional differential equations. Fractional operators, in contrast to traditional integer-order models, inherently take into account the impact of previous states on current dynamics, offering a more accurate depiction of several physical, biological, and engineering processes. Fractional formulations have proven to be more flexible in capturing anomalous diffusion, long-term persistence, and diverse interactions that traditional models are unable to fully capture in epidemiology and related applied sciences. Fractional differential equations with the Caputo derivative are commonly utilized because of their straightforward physical interpretation and ability to accommodate classical beginning conditions represented in integer-order derivatives [27,28,29]. The Atangana–Baleanu derivative, which uses a non-singular Mittag-Leffler kernel to more realistically explain fading memory, was recently introduced as an extension of the Caputo framework. This feature provides better numerical stability and smoother dynamics while overcoming the drawbacks of solitary kernels [30,31,32,33]. By concurrently combining geometric complexity through the fractal dimension and memory effects through the fractional order, fractal–fractional derivatives further improve modeling capability. Because of this dual structure, fractal–fractional models are able to represent the spatial or structural heterogeneity and temporal persistence that are present in many physical and biological systems. Because ordinary integer-order or single-order fractional models are unable to fully describe complicated dynamical processes, the combination of ABC-type operators with fractal–fractional formulations provides a reliable and adaptable mathematical framework [34,35,36,37].

The motivation of this paper lie in investigating optimal strategies for halting the spread of both diseases through the development of a mathematical model for cholera and Buruli ulcer co-infection incorporating five distinct control measures. This framework provides new insights into the coupled transmission dynamics and is expected to motivate further analytical and epidemiological studies. Building upon the proposed co-infection framework, the model is further analyzed through a rigorous stability investigation based on functional analysis. Approximate solutions are obtained using iterative numerical techniques in combination with the Adams–Bashforth scheme. In addition, a deep neural network–based computational approach is employed for the fractional system, where two hidden layers consisting of 50 and 5 neurons, respectively, are implemented. The integration of deep neural networks with fractional calculus provides an effective framework for addressing complex mathematical and physical models that are often challenging for conventional numerical approaches. Accordingly, key aspects of the proposed model, including accuracy, numerical stability, enhanced precision, and reduced computational errors compared with classical numerical methods, are examined in detail.

2 Model formulation

This part aims to develop a mathematical equation that demonstrates the co-dynamics of cholera and Buruli ulcer (BU). In this context, we denote the total individuals by N_h which is further divided into several compartments: susceptible individuals S_h; those infected with Buruli ulcer only I_b; those who infected with cholera only I_c; individuals co-infected with both diseases D_{bc}; individual who are recovered from Buruli ulcer only R_b; those who recover from cholera only R_c and individuals who have recovered from both cholera and Buruli ulcer R_{bc}. Thus N_h=$S_h + I_b + I_c + D_{bc} + R_b + R_c + R_{bc}$. The vector population is represented by N_v, and the susceptible and infected water-bugs are represented by S_v and I_v, respectively, using the formula N_v=$S_v + I_v$. The co-infection paradigm for cholera and BU is considered from the literature [38] and is as follows:

$$
\begin{aligned}
{}^{\mathrm{FFC}}\mathrm{D}^{\tau,\kappa}S_h(t) &= \pi_h + \phi R_b + \Psi R_c + \theta R_{bc} - \left(\beta_h I_v + \beta_l\right) S_h - \mu_h S_h \\
{}^{\mathrm{FFC}}\mathrm{D}^{\tau,\kappa}I_b(t) &= \beta_v I_v S_h - \beta_l I_b - \left(\eta + \mu_h + \kappa\right) I_b \\
{}^{\mathrm{FFC}}\mathrm{D}^{\tau,\kappa}I_c(t) &= \beta_l S_h - \beta_h I_v I_c - \left(\delta + \mu_h + I\right) I_c \\
{}^{\mathrm{FFC}}\mathrm{D}^{\tau,\kappa}D_{bc}(t) &= \beta_h I_v I_c + \beta_l I_b - \left(\delta + \mu_h + \gamma + \varpi\right) D_{bc} \\
{}^{\mathrm{FFC}}\mathrm{D}^{\tau,\kappa}R_b(t) &= \eta I_b - \left(\phi + \mu_h\right) R_b + \varepsilon(1-\delta) D_{bc} \\
{}^{\mathrm{FFC}}\mathrm{D}^{\tau,\kappa}R_c(t) &= \rho I_c - \left(\Psi + \mu_h\right) R_c + (1-\varepsilon)(1-\delta) D_{bc} \\
{}^{\mathrm{FFC}}\mathrm{D}^{\tau,\kappa}R_{bc}(t) &= \delta D_{bc} - \left(\theta + \mu_h\right) R_{bc} \\
{}^{\mathrm{FFC}}\mathrm{D}^{\tau,\kappa}B(t) &= \omega\left(I_c - \rho D_{bc}\right) - \mu_h B \\
{}^{\mathrm{FFC}}\mathrm{D}^{\tau,\kappa}S_v(t) &= \pi_v - \beta_v\left(I_b + D_{bc}\right) S_v - \mu_v S_v \\
{}^{\mathrm{FFC}}\mathrm{D}^{\tau,\kappa}I_v(t) &= \beta_v\left(I_b + D_{bc}\right) S_v - \mu_v I_v
\end{aligned}
\tag{1}
$$

Here, the likelihood of contracting cholera, represented by β_1, is given by the expression β_1=$\frac{zB}{K+B}$, where 'B' stands for the bacterial population, 'z' is the ingestion rate, and 'K' represents the concentration of Mycobacterium ulcerous in the water. The pace at which healthy individuals are recruited is represented by the symbol λ_h. The rate of human-Mycobacterium ulcerans contact is indicated by the parameter λ. Furthermore, l and γ represent the cholera-related death rates. The symbols β_h and β_v for the likelihood of acquiring BU in humans, and water-bugs respectively. Probability of individuals developing Buruli ulcer is denoted by β_h, while the corresponding fatality rates associated with Buruli ulcer are denoted by 'k' and ϖ. The average amount of contamination that each cholera-infected person contributes to the aquatic environment is indicated by the parameter ω. The corresponding rates at which immunity declines are represented by ϕ, Ψ and θ, while η, ρ, and δ denote the recovery rates, respectively. Where $\varepsilon(1-\delta)$ represent those individuals, which are infected with both the diseases but recovered only from Buruli ulcer, whereas $(1-\varepsilon)(1-\delta)$ represent those individuals which are infected with both diseases and recovered only from cholera. μ_h and μ_v represent human and water bugs morality rate and ρ deal deals with modification parameters, where the chances of water-bugs receiving infection with Buruli ulcer is β_v and μ_b are death rates of bacteria. People that re-enter the transmission cycle as a result of immunity loss or incomplete recovery are represented by the secondary susceptible and infected compartments. This phenomenon is frequently seen in areas where cholera is endemic and in populations affected by Buruli ulcers. The persistence of infections in aquatic environments is captured by the environmental reservoir compartment, which is crucial for maintaining cholera epidemics and promoting Mycobacterium ulcerans indirect transmission. Therefore,

physiologically established reinfection pathways and environmentally driven transmission mechanisms are reflected in the interaction terms connecting these compartments.

3 Basic definitions

Definition: [41] Let us suppose a continuous function $\mathscr{P}(t), t \in [a,b]$ and differentiable in (a, b), then the fractal fractional derivative of order δ and dimension β is defined as

$$^{FF}\mathbf{D}_t^{\delta,\beta}\mathscr{P}(t) = \frac{1}{(m-\delta)}\frac{d}{dt^{\beta}}\int_0^t (t-y)^{m-\delta-1}\mathscr{P}(y)dy, \tag{2}$$

for $m-1 < \delta, \beta \leq m, m \in \mathrm{N}$ and $\frac{d\mathscr{P}(y)}{dy^{\beta}} = \lim_{t\to 0}\left(\frac{\mathscr{P}(t)}{t^{\beta}-y^{\beta}} - \frac{\mathscr{P}(y)}{t^{\beta}-y^{\beta}}\right)$.

Definition: [41] let suppose a continuous-function $\mathscr{P}(t)$, where t between 'a' and 'b' then the integration of fractal fractional of fractional order δ is define as

$$^{FF}\mathbf{I}^{\delta}\mathscr{P}(t) = \frac{\beta}{\Gamma(\delta)}\int_0^t (t-y)^{\delta-1}y^{\beta-1}\mathscr{P}(y)dy. \tag{3}$$

Definition:[41] The proposed system (1) shows the Ulam Hayers stability, for real value $\mathscr{G}_{\delta,\beta} \geq 0$ such as $\forall\ \vartheta > 0$ and all the roots $\varphi \in C^1(\mathscr{X},\mathbf{R})$, then

$|^{FF}\mathbf{D}^{\delta,\beta}\varphi(\mathrm{t}) - \Pi(t,\varphi(t))| \leq \vartheta, \quad t \in \mathscr{X},$

$\mathscr{Y} \in C^1(\mathscr{X},\mathbf{R})$ has only one solution of model (1), $\ni$

$|\varphi(t) - \mathscr{Y}(t)| \leq \mathscr{G}_{\delta,\beta}, \quad t \in \mathscr{X},$

Definition: [27] For a differentiable function $f(t) \in H^1$ in (a,b), the Caputo derivative is define as

$$^{C}_{a}D_t^{\delta} = \frac{1}{\Gamma(n-\delta)}\int_a^x f^n(\zeta)(t-\zeta)^{n-(\delta+1)}d\zeta, \quad for\ \ n-1 < \delta < n \tag{4}$$

$$^{C}_{a}D_t^{\delta} = \frac{d^n f(t)}{dt^n}, \quad for \quad \delta = n,$$

where $b > a$, and $\delta \in [0,1]$. And $\Gamma(.)$ is the gamma function, and define as

$$\Gamma(n) = \int_0^{\infty} \Psi^{x-1}e^{-\Psi}d\Psi, \quad 0 < Re(x). \tag{5}$$

Note: For qualitative analysis of the proposed system, we consider a Banach-space $\mathrm{U} = X \times X \times X \times X$ where $X = \mathscr{G}(X)$ with norm: $\|\chi(t)\| = \|S_h, I_b, I_c, D_{bc}, R_b, R_c, R_{bc}, B\| = \max_{t\in[0,T]}\left\{|S_h|, |I_b|, |I_c|, |D_{bc}|, |R_b|, |R_c|, |R_{bc}|, |B|\right\}$.

4 Qualitative analysis

The original fractal-fractional system can be recast as an analogous integral equation thanks to the operator formulation. While equicontinuity assures smooth temporal behavior, boundedness guarantees that solutions stay inside a biologically significant range. For epidemiological predictions to be reliable, the contraction condition verifies that the system allows a unique and stable solution under slight perturbations. Here, we investigate whether a solution to the given model (1), exists and whether it is unique.

4.1 Existence

Nonlinear and nonlocal behavior characterized the proposed model (1). Exact method for finding the roots of a nonlinear systems do not generally exist. However, in rare situations, an exact solution may be possible. In this context, the principle

of functional analysis are used to check whether the given system has a solution. The R.H.S of the proposed model (1), we have the selected integral being differentiable as

$$
\begin{aligned}
{}^{\mathrm{RL}}\mathrm{D}^{\tau,\kappa}S_h(t) &= \kappa^{\kappa-1}\Lambda_1(S_h,I_b,I_c,D_{bc},R_b,R_c,R_{bc},S_v,I_v,B,t) = \pi_h+\phi R_b+\Psi R_c+\theta R_{bc}-\Big(\beta_h I_v+\beta_l\Big)S_h-\mu_h S_h\\
{}^{\mathrm{RL}}\mathrm{D}^{\tau,\kappa}I_b(t) &= \kappa^{\kappa-1}\Lambda_2(S_h,I_b,I_c,D_{bc},R_b,R_c,R_{bc},S_v,I_v,B,t) = \beta_v I_v S_h-\beta_l I_b-\Big(\eta+\mu_h+\kappa\Big)I_b\\
{}^{\mathrm{RL}}\mathrm{D}^{\tau,\kappa}I_c(t) &= \kappa^{\kappa-1}\Lambda_3(S_h,I_b,I_c,D_{bc},R_b,R_c,R_{bc},B,t) = \beta_l S_h-\beta_h I_v I_c-\Big(\delta+\mu_h+I\Big)I_c\\
{}^{\mathrm{RL}}\mathrm{D}^{\tau,\kappa}D_{bc}(t) &= \kappa^{\kappa-1}\Lambda_4(S_h,I_b,I_c,D_{bc},R_b,R_c,R_{bc},S_v,I_v,B,t) = \beta_h I_v I_c+\beta_l I_b-\Big(\delta+\mu_h+\gamma+\varpi\Big)D_{bc}\\
{}^{\mathrm{RL}}\mathrm{D}^{\tau,\kappa}R_b(t) &= \kappa^{\kappa-1}\Lambda_5(S_h,I_b,I_c,D_{bc},R_b,R_c,R_{bc},S_v,I_v,B,t) = \eta I_b-\Big(\phi+\mu_h\Big)R_b+\varepsilon(1-\delta)D_{bc}\\
{}^{\mathrm{RL}}\mathrm{D}^{\tau,\kappa}R_c(t) &= \kappa^{\kappa-1}\Lambda_6(S_h,I_b,I_c,D_{bc},R_b,R_c,R_{bc},S_v,I_v,B,t) = \rho I_c-\Big(\Psi+\mu_h\Big)R_c+(1-\varepsilon)(1-\delta)D_{bc}\\
{}^{\mathrm{RL}}\mathrm{D}^{\tau,\kappa}R_{bc}(t) &= \kappa^{\kappa-1}\Lambda_7(S_h,I_b,I_c,D_{bc},R_b,R_c,R_{bc},S_v,I_v,B,t) = \delta D_{bc}-\Big(\theta+\mu_h\Big)R_{bc}\\
{}^{\mathrm{RL}}\mathrm{D}^{\tau,\kappa}B(t) &= \kappa^{\kappa-1}\Lambda_8(S_h,I_b,I_c,D_{bc},R_b,R_c,R_{bc},S_v,I_v,B,t) = \omega\Big(I_c-\rho D_{bc}\Big)-\mu_h B\\
{}^{\mathrm{RL}}\mathrm{D}^{\tau,\kappa}S_v(t) &= \kappa^{\kappa-1}\Lambda_9(S_h,I_b,I_c,D_{bc},R_b,R_c,R_{bc},S_v,I_v,B,t) = \pi_v-\beta_v\Big(I_b+D_{bc}\Big)S_v-\mu_v S_v\\
{}^{\mathrm{RL}}\mathrm{D}^{\tau,\kappa}I_v(t) &= \kappa^{\kappa-1}\Lambda_{10}(S_h,I_b,I_c,D_{bc},R_b,R_c,R_{bc},S_v,I_v,B,t) = \beta_v\Big(I_b+D_{bc}\Big)S_v-\mu_v I_v
\end{aligned}
\tag{6}
$$

We may write the proposed system for $t\in\Lambda$, as

$$
\begin{aligned}
{}^{\mathscr{RL}}\mathrm{D}^{\tau}\varphi(t) &= \kappa t^{\kappa-1}\varphi(t,\varphi(t)),\quad 0<\tau,\kappa\le 1,\\
\varphi(0) &= \varphi_0.
\end{aligned}
\tag{7}
$$

By replacing ${}^{\mathscr{RL}}\mathrm{D}^{\tau,\kappa}$ by ${}^{\mathscr{C}}\mathrm{D}^{\tau,\kappa}$, using the Riemann-Liouville integral, the solution of (7) will be obtain as of the form

$$
\varphi(t)=\varphi_0(t)+\frac{\kappa}{\Gamma(\tau)}\int_0^t y^{\kappa-1}(t-y)^{\tau-1}\chi(y,\varphi(y))dy,
\tag{8}
$$

for relation

$$
\begin{aligned}
\varphi(t) &= \Big(S_h(t),I_b(t),I_c(t),D_{bc}(t),R_b(t),R_c(t),R_{bc}(t),S_v(t),I_v(t),B(t)\Big)^T\\
\varphi_0(t) &= \Big(S_h(0),I_b(0),I_c(0),D_{bc}(0),R_b(0),R_c(0),R_{bc}(0),S_v(0),I_v(0),B(0)\Big)^T.\\
\chi(t,\varphi(t)) &= \Big(\Lambda_j(S_h,I_b,I_c,D_{bc},R_b,R_c,R_{bc},S_v,I_v,B,t)\Big)^T,\quad j=1,2,..,10.
\end{aligned}
\tag{9}
$$

Here, now we can change the proposed problem (1), to a invariant point state with $\blacksquare:\mathscr{C}\to\mathscr{C}$ operator, is defined as

$$
\Omega(\varphi)(t)=\varphi_0(t)+\frac{\kappa}{\Gamma(\tau)}\int_0^t y^{\kappa-1}(t-y)^{\tau-1}\chi(y,\varphi(y))dy.
\tag{10}
$$

For the proposed model we find the existence results using the below theorem.

Theorem 1.*[42] For the defined operator $\Omega : \mathscr{C} \to \mathscr{C}$, the mapping is completely-continuous if* $\mathrm{J}(\Omega) = \big(\varphi \in \mathscr{C} : \varphi = \tau\Omega(\varphi),\ \tau \in (0,1)\big)$*, is bounded, implies that* Ω *has at-least one invariant-point in* $\mathscr{C}$.

Theorem 2.*Let* $\chi : \Xi \times \mathscr{C} \to \mathrm{R}$ *be a continuous mapping, then* Ω *has the properties of compactness.*

*Proof.*First we have to check the continiuity of operator $\Omega : \mathscr{C} \to \mathscr{C}$ in Eq. (8). We consider $\mathscr{C}$ has a bounded-subset E, then $\exists$, $\mathscr{H}_\chi > 0$ with $|\chi(t,\varphi(t))| \leq \mathscr{H}_\chi, \forall\ \varphi \in \mathrm{E}$. For any $\varphi \in \mathrm{E}$, we have

$$\begin{aligned}\|\Omega(\varphi)\| &\leq \frac{\kappa\mathscr{H}_\chi}{\Gamma(\rho)} \max_{t\in(0,T)} \left| \int_0^t (\tau - y)^{\tau-1} y^{\kappa-1} dy \right| \\ &\leq \frac{\kappa\mathscr{H}_\chi}{\Gamma(\tau)} \max_{t\in(0,T)} \int_0^t (1-z)^{\kappa-1} z^{\tau-1} t^{\tau+\kappa-1} dz \\ &\leq \frac{\kappa\mathscr{H}_\chi T^{\tau+\kappa-1}}{\Gamma(\tau)} \mathrm{E}(\tau,\kappa). \end{aligned} \tag{11}$$

Hence equation (11), varifies that Ω is bounded uniformly, and $\mathrm{E}(\tau,\kappa)$ donote a Beta-function. Moreover, we check the equicontinuity of the operator $\Omega, \forall\ t_1, t_2 \in \Xi$ and $\Psi \in \mathrm{E}$, we have

$$\begin{aligned}\|\Omega(\Psi(t_1)) - \Omega(\varphi(t_2))\| &\leq \frac{\kappa\mathscr{H}_\varphi}{\Gamma(\tau)} \max_{t\in(0,T)} \left| \int_0^{t_1} (t_1 - y)^{\tau-1} y^{\kappa-1} dy - \int_0^{t_2} (t_2 - y)^{\tau-1} y^{\kappa-1} dy \right| \\ &\leq \frac{\kappa\mathscr{H}_\varphi \mathrm{E}(\tau,\kappa)}{\Gamma(\tau)} (t_1^{\tau+\kappa-1} - t_2^{\tau+\kappa-1}) \to 0 \quad as \quad t_1 \to t_2. \end{aligned}$$

Which shows that Ω is equicontinuous, hence Ω is bounded and continuous also, so, by "Arzel*á*-Ascoli" theorem, Ω is relatively compact and also completely continuous. Now we utilize the hypothesis

(a) A constant $M_\chi > 0$ exists, such that for every $\varphi, \bar{\varphi} \in \mho$ we have

$$\Big|\chi(t,\varphi) - \chi(t,\bar{\varphi})\Big| \leq \mathrm{M}_\chi \Big|\varphi\Big| - \Big|\bar{\varphi}\Big|.$$

4.2 Existence of Unique solution

With the help of fixed-point theory. [42], we have to check the uniqueness of the solution for model (1).

Theorem 3.*The proposed system* (1)*, has one and-only-one root, by applying hypothesis* (a) *for* $\beta < 1$ *as*

$$\kappa = \frac{\kappa M_\chi \Omega^{\tau+\kappa-1}(E(\tau,\kappa))}{\Gamma(\tau)}. \tag{12}$$

*Proof.*Let $\max_{0<t<T} |\chi(t,0)| = \mathscr{V}_\chi < \infty$, such that

$$\frac{\kappa T^{\tau+\kappa-1}\big(E(\tau,\kappa)\big)\mathscr{V}_\varphi}{\Gamma(\tau) - \kappa T^{\tau+\kappa-1}\big(E(\tau,\kappa)\big)M_\chi} \leq r, \tag{13}$$

here we have to show $\Omega(E_r)$ is a subset of E_r and $E_r = \big\{\varphi \in \mathscr{V} : ||\varphi|| \leq r\big\}$, for $\chi \in E_r$, so we have

$$\begin{aligned}\|\Omega(\varphi)\| &\leq \frac{\kappa}{\Gamma(\tau)} \max_{0<t<T} \int_0^t y^{\kappa-1}(t-y)^{\tau-1} \big(|\chi(t,\varphi(t)) - \chi(t,0)| + |\chi(t,0)|\big) dy \\ &\leq \frac{\kappa\Omega^{\tau+\kappa-1}\mathrm{E}(\tau,\kappa)(\mathrm{M}_\chi\|\chi| + \mathscr{V}_\chi)}{\Gamma(\tau)} \\ &\leq \frac{\kappa\Omega^{\tau+\kappa-1}\mathrm{E}(\tau,\kappa)(\mathrm{M}_\chi r + \mathscr{V}_\chi)}{\Gamma(\tau)} \\ &\leq r. \end{aligned}$$

According to equation (10), where we have Ω and using hypothesis (a) for all $t \in \Xi, \varphi, \overline{\mathscr{W}} \in \Xi$, we get

$$\begin{aligned}\|\Omega(\varphi) - \Omega(\overline{\mathscr{W}})\| &\leq \frac{\kappa}{\Gamma(\tau)} \max_{0<t<T]} \left| \int_0^t y^{\kappa-1}(t-y)^{\tau-1} \chi(y,\chi(y)) dy - \int_0^t y^{\kappa-1}(t-y)^{\kappa-1} \chi(y,\overline{\chi}(y)) dy \right| \\ &\leq \beta\|\chi - \overline{\mathscr{W}}\|. \end{aligned} \tag{14}$$

So, the Ω has a contraction by using equation (14). Hence, equation (8), has a unique solution which implies the system (1) has a unique solution.

4.3 Ulam-Hyers (UH) Stability Analysis

The Ulam-Hyers type stability analysis for the problem (1), we use functional analysis. For this we take $\vartheta(0) = 0$ i.e., ϑ is independent and $\vartheta \in C(\Xi)$, then

– $|\vartheta(t)| \leq \alpha$, for $\alpha > 0$;
– ${}^{FF}\mathrm{D}_t^{\tau,\kappa}\varphi(t) = \vartheta(t,\varphi(t)) + \vartheta(t)$.

Lemma 1.*For the perturb equation, the solution is*

$$\begin{aligned} {}^{FF}\mathrm{D}^{\tau,\kappa}\varphi(t) &= \vartheta(t,\varphi(\mathrm{t})) + \vartheta(t) \\ \varphi(0) &= \varphi_0, \end{aligned} \tag{15}$$

Which satisfying

$$\begin{aligned} \left|\varphi(t) - \left(\vartheta_0(t) + \frac{\beta}{\Gamma(\tau)}\int_0^t y^{\kappa-1}(t-y)^{\tau-1}\vartheta(y,\vartheta(y))\right)\right| &\leq \left(\frac{\kappa \mathrm{T}^{\tau+\kappa-1}E(\tau,\kappa)}{\Gamma(\tau)}\right)\varepsilon \\ &= \mathrm{C}_{\tau,\kappa}\varepsilon. \end{aligned} \tag{16}$$

Theorem 4.*From (16), with (a), the proposed system's solution is Ulam-Hyers stable, so the recieved result for the proposed model is Ulam-Hyers stable, when $\kappa < 1$, and κ is in (12).*

*Proof.*Let the unique solution $\mathscr{G} \in \mathscr{C}$ and $\varphi \in \mathscr{C}$ are solutions of equation (8), further we use fractal-fractional integral, we define in (3), we get

$$\begin{aligned} |\varphi(t) - \mathscr{G}(t)| &= \left|\varphi(t) - \left(\mathscr{G}_0(t) + \frac{\kappa}{\Gamma(\tau)}\int_0^t (t-y)^{\rho-1}y^{\kappa-1}\vartheta(y,\mathscr{G}(y))dy\right)\right| \\ &\leq \left|\varphi(t) - \left(\varphi_0(t) + \frac{\kappa}{\Gamma(\tau)}\int_0^t (t-y)^{\tau-1}y^{\kappa-1}\vartheta(y,\varphi(y))dy\right)\right| \\ &+ \left|\left(\varphi_0(t) + \frac{\kappa}{\Gamma(\tau)}\int_0^t (t-y)^{\tau-1}y^{\kappa-1}\vartheta(y,\varphi(y))dy\right)\right. \\ &- \left.\left(\mathscr{G}_0(t) + \frac{\kappa}{\Gamma(\tau)}\int_0^t (t-y)^{\tau-1}y^{\kappa-1}\vartheta(y,\mathscr{G}(y))dy\right)\right| \\ &\leq \mathrm{C}_{\tau,\kappa}\varepsilon + \frac{\kappa \mathrm{T}^{\tau+\kappa-1}\mathrm{M}_\varphi}{\Gamma(\tau)}E(\tau,\kappa)\|\varphi - \mathscr{G}\| \\ &\leq \mathrm{C}_{\tau,\kappa} + \kappa\|\varphi - \mathscr{G}\|, \end{aligned}$$

hence

$$\|\varphi - \mathscr{G}\| \leq \mathrm{C}_{\tau,\kappa} + \kappa\|\varphi - \mathscr{G}\|. \tag{17}$$

Equation (17), may written as

$$\|\varphi - \mathscr{G}\| \leq \left(\frac{\mathrm{C}_{\tau,\kappa}}{1-\kappa}\right)\varepsilon. \tag{18}$$

The obtained bound demonstrates that small perturbations in the system lead only to proportionally small deviations in the solution, confirming the Ulam–Hyers stability of the proposed model. Hence, from equation (18), holding all the constrants of Ulam-Hyers stability, so we claime that equation (8), has stable solution.

5 Approximate solution

In this part, the approximate solution of the proposed model (1) will be calculated under the numerical iterative scheme, the fractional Adams Bashforth method [43]. For this we may write the given system as

$$
\begin{aligned}
{}^{FF}\mathrm{D}^{\tau,\kappa}S_h(t) &= \mathscr{P}_1\big(S_h(t),t\big) = \pi_h + \phi R_b + \Psi R_c + \theta R_{bc} - \Big(\beta_h I_v + \beta_l\Big) S_h - \mu_h S_h \\
{}^{FF}\mathrm{D}^{\tau,\kappa}I_b(t) &= \mathscr{P}_2\big(I_b(t),t\big) = \beta_v I_v S_h - \beta_l I_b - \Big(\eta + \mu_h + \kappa\Big) I_b \\
{}^{FF}\mathrm{D}^{\tau,\kappa}I_c(t) &= \mathscr{P}_3\big(I_c(t),t\big) = \beta_l S_h - \beta_h I_v I_c - \Big(\delta + \mu_h + I\Big) I_c \\
{}^{FF}\mathrm{D}^{\tau,\kappa}D_{bc}(t) &= \mathscr{P}_4\big(D_{bc}(t),t\big) = \beta_h I_v I_c + \beta_l I_b - \Big(\delta + \mu_h + \gamma + \varpi\Big) D_{bc}
\end{aligned}
$$

$$
\begin{aligned}
{}^{FF}\mathrm{D}^{\tau,\kappa}R_b(t) &= \mathscr{P}_5\big(R_b(t),t\big) = \eta I_b - \Big(\phi + \mu_h\Big) R_b + \varepsilon(1-\delta) D_{bc} \\
{}^{FF}\mathrm{D}^{\tau,\kappa}R_c(t) &= \mathscr{P}_6\big(R_c(t),t\big) = \rho I_c - \Big(\Psi + \mu_h\Big) R_c + (1-\varepsilon)(1-\delta) D_{bc} \\
{}^{FF}\mathrm{D}^{\tau,\kappa}R_{bc}(t) &= \mathscr{P}_7\big(R_{bc}(t),t\big) = \delta D_{bc} - \Big(\theta + \mu_h\Big) R_{bc} \\
{}^{FF}\mathrm{D}^{\tau,\kappa}B(t)(t) &= \mathscr{P}_8\big(B(t),t\big) = \omega\Big(I_c - \rho D_{bc}\Big) - \mu_h B \\
{}^{FF}\mathrm{D}^{\tau,\kappa}S_v(t) &= \mathscr{P}_9\big(S_v(t),t\big) = \pi_v - \beta_v\Big(I_b + D_{bc}\Big) S_v - \mu_v S_v \\
{}^{FF}\mathrm{D}^{\tau,\kappa}I_v(t) &= \mathscr{P}_{10}\big(I_v(t),t\big) = \beta_v\Big(I_b + D_{bc}\Big) S_v - \mu_v I_v. \qquad (19)
\end{aligned}
$$

With

$$
\begin{aligned}
S_h(t) &= S_h(0) + \frac{\kappa}{\Gamma(\tau)} \int_0^t x^{\kappa-1}(t-y)^{\tau-1} \mathscr{P}_1(S_h,y)dy \\
I_b(t) &= I_b(0) + \frac{\kappa}{\Gamma(\tau)} \int_0^t x^{\kappa-1}(t-y)^{\tau-1} \mathscr{P}_2(I_b,y)dy \\
I_c(t) &= I_c(0) + \frac{\kappa}{\Gamma(\tau)} \int_0^t x^{\kappa-1}(t-y)^{\tau-1} \mathscr{P}_3(I_c,y)dy \\
D_{bc}(t) &= D_{bc}(0) + \frac{\kappa}{\Gamma(\tau)} \int_0^t x^{\kappa-1}(t-y)^{\tau-1} \mathscr{P}_4(D_{bc},y)dy \\
R_b(t) &= R_b(0) + \frac{\kappa}{\Gamma(\tau)} \int_0^t x^{\kappa-1}(t-y)^{\tau-1} \mathscr{P}_5(R_b,y)dy \\
R_c(t) &= R_c(0) + \frac{\kappa}{\Gamma(\tau)} \int_0^t x^{\kappa-1}(t-y)^{\tau-1} \mathscr{P}_6(R_c,y)dy \\
R_{bc}(t) &= R_{bc}(0) + \frac{\kappa}{\Gamma(\tau)} \int_0^t x^{\kappa-1}(t-y)^{\tau-1} \mathscr{P}_7(R_{bc},y)dy
\end{aligned}
$$

$$B(t) = B(0) + \frac{\kappa}{\Gamma(\tau)} \int_0^t x^{\kappa-1}(t-y)^{\tau-1} \mathscr{P}_8(B,y)dy$$
$$S_v(t) = S_v(0) + \frac{\kappa}{\Gamma(\tau)} \int_0^t x^{\kappa-1}(t-y)^{\tau-1} \mathscr{P}_9(S_v,y)dy$$
$$I_v(t) = I_v(0) + \frac{\kappa}{\Gamma(\tau)} \int_0^t x^{\kappa-1}(t-y)^{\tau-1} \mathscr{P}_10(I_v,y)dy. \tag{20}$$

For the approximate solution of equation (20), utilizing the advance iterative method t_{1+k}. Solution for the first class of the proposed model, the obtain integral is as

$$S_{h(1+k)}(t) = S_h(0) + \frac{\kappa}{\Gamma(\tau)} \sum_{\alpha=0}^{k} \int_{t_\alpha}^{t_{(k+1)}} x^{\kappa-1}(t_{(k+1)}-y)^{\tau-1} \mathscr{P}_1(S_h,y)dy. \tag{21}$$

For all the values of $[t_\alpha, t_{1+\alpha}]$ in Lagrange-interpolation polynomial with function $\mathscr{P}_1(S_h,y)$ along with $= [t_\alpha - t_{-1+\alpha}]$, such that

$$S_{h(k)}^{\circledast} \approx \frac{\left[(t-t_{\alpha-1})t_\alpha^{\beta-1}\mathscr{P}_1(\mathscr{A}_{(\alpha)},t_\alpha) - (t-t_\alpha)t_{\alpha-1}^{\kappa-1}\mathscr{P}_1(\mathscr{A}_{(\alpha-1)},t_{\alpha-1})\right]}{}, \tag{22}$$

plugging equation (22) in equation (21) we obtain

$$S_{h[k+1]} = S_h(0) + \frac{\kappa}{\Gamma(\tau)} \sum_{j=0}^{k} \int_{t_j}^{t_{j+1}} y^{\kappa-1}(t_{k+1}-y)^{\tau-1} S_{h_k}^{\circledast} dy. \tag{23}$$

The integral equation (23) in right hand side give the solution for class $S_h(t)$ of the proposed model by using FF derivative with Caputo operator.

$$\begin{aligned} S_{h[1+k]} = S_h(0) + \frac{\kappa^\tau}{\Gamma(\tau+2)} \sum_{\alpha=0}^{k} \Bigg[& t_\alpha^{\kappa-1}\mathscr{P}_1(S_{h(\alpha)},t_\alpha) \\ & \times \Big((1+k-\alpha)^\kappa(2+k+\kappa-\alpha) - (k-\alpha)^\kappa(2+k+2\kappa-\alpha)\Big) \\ & - t_{\alpha-1}^{-1+\kappa}\mathscr{P}_1(S_{h(-1+\alpha)},t_{-1+\alpha})\Big((1-\alpha+k)^\kappa + 1 - k + \alpha)^\kappa(k-\alpha+1+\kappa)\Big)\Bigg], \end{aligned} \tag{24}$$

similarly, the remaining terms are

$$\begin{aligned} \mathscr{F}_{[1+k]} = \mathscr{F}(0) + \frac{\kappa^\tau}{\Gamma(\tau+2)} \sum_{\alpha=0}^{k} \Bigg[& t_\alpha^{\kappa-1}\mathscr{P}_2(\mathscr{F}_{(\alpha)},t_\alpha) \\ & \times \Big((1-\alpha+k)^\kappa(2+k-\alpha+\kappa) - (k-\alpha)^\kappa(2-\alpha+k+2\kappa)\Big) \\ & - t_{-1+\alpha}^{\kappa-1}\mathscr{P}_2(\mathscr{F}_{(\alpha-1)},t_{\alpha-1})\Big((1+k-\alpha)^\kappa + 1 + (\alpha-k)^\kappa(k-\alpha+1+\kappa)\Big)\Bigg], \end{aligned} \tag{25}$$

$$\begin{aligned} mathcalU_{[1+k]} = \mathscr{U}(0) + \frac{\kappa^\tau}{\Gamma(\tau+2)} \sum_{\xi=0}^{k} \Bigg[& t_\alpha^{-1+\kappa}\mathscr{P}_3(\mathscr{U}_{(\alpha)},t_\alpha) \\ & \times \Big((1-\alpha+k)^\kappa(2-\alpha+k+\kappa) - (k-\alpha)^\beta(2-\alpha+k+2\kappa)\Big) \\ & - t_{\alpha-1}^{-1+\kappa}\mathscr{P}_3(\mathscr{U}_{(-1+\alpha)},t_{(-1+\alpha)})\Big((1-\alpha+k)^\kappa + 1 + (\alpha-k)^\kappa(k-\alpha+1+\kappa)\Big)\Bigg]. \end{aligned} \tag{26}$$

6 Simulations with Deep Neural Network

This section of manuscript, MATLAB is used for the simulations of the obtain analytical results. The validity and efficiency of the numerical result for the co-dynamics of Buruli Ulcer and cholera applying the FFC operator, are verified

by numerical simulations. The evoluation of each class for the proposed model are provided for few sets of fractional-order τ and the fractal-dimension κ. Initial values are compared for each class, where fractional-order and fractional-dimension are compare, which are presented as $\tau, \kappa = 0.70, 0.80, 0.90, 1.00$ in this simulations. Using fractional Adams Bashforth method to solve the Buruli Ulcer and Cholera model semi-analytically for test, the validity, and feasibility data sets. For each fractional value there is a different representation of dynamics in the model, which shows efficiency of fractional derivative as compared to the integer order derivatives.

The deep neural network was trained using the Adam optimizer with a learning rate of $10^{-}3$. The network was trained for 1000 epochs, and convergence was monitored through the reduction of the mean squared error. Early stopping was employed to prevent overfitting, with training terminated once the validation loss ceased to improve. The DNN method is considered for the model with two hidden lyers 50 and 5 neurons respectively. The first lyer shows the tangent hyperbolic activation and the second lyer shows linear activations function. The data set is used for different fractional orders and devided it into three diffirent categeries with 70% training, 15% testing, and 15% validation.

The dynamics of $S_h(t)$ with the help of DNN is obtained in Fig: 1a, which represent the approximate regression coefficient (RC) 1. The mean error (ME) is $4.8512e-08$ and root mean square (RMS) error is 0.00022025. We observe that the scheme has ME $2.0774e-07$ and the varience error $-2.0774e-07$, from the histogram. Utilized same teqniques for the train data for the result in 1b, where the RC is 1, the ME is $4.8521e-08$ and the RMS error is 0.00022026 From the histogram the ME is $-5.665e-07$ and the varience error is 0.00022028. In 1c, we focus on the test data the RC is 1, the mean and RMS errors are $4.909e-08$ and 0.00022156 respectively, which shows the high accuracy of the DNN scheme. Similarly, the ME is $-8.6393e-07$ and the RMS error is 0.00022156 which are conform from the histogram. In Fig: 1d, the validation data is plotted, the RC is 1, the ME is $4.7893e-08$ and the RMS error is 0.00021884 In the histogram the ME is $2.1227e-06$ and the varience error is 0.00021884. All the aspects of proposed model, accuracy, remarkable precision, and reducing computational errors compared to classical numerical techniques of the method are explored comprehensivly. Fractional order and machine systems can be used to compress first class dynamics, as shown in 1e. The absolute error is presented in 1f. Combining DNN with fractinal calculus introduces a novel framework for solving complex mathematical and physical problems that traditoinal methods often struggle with.

The graphical representation of class $I_b(t)$ with the add of deep Neural network in Fig:2a. Here, we observe that the approximate RC is 1, the mean and RMS error are $9.2954e-07$ and 0.00096412 respectively. We also note that from the histogram the maen error is $4.8125e-06$ and the varience error is 0.00096412. Utilizing the said method for the train data we get the graphs in 2b. From the graph we see that the RC is 1, the maen and RMS errors are $9.2783e-07$ and 0.00096324 respectively. From the histogram plotting we see that the ME is $6.0713e-06$ and the varience error is 0.00096323. In 2c, with the help of deep Neural network the test data is presented graphycall. The regression coefficinet is 1, ME and RMS error are $9.3288e-07$ and 0.00096586 respectively. In histogram, the ME and varience error $3.4812e-06$ and 0.00096587 respectively. In 2d we see that the validation regression analysis is 1, maen erroer and RMS error are $9.3413e-07$ and 0.00096651. From the histigram we confirm that the ME is $2.6946e-07$ and the varience error is 0.00096652. Fractional order and deep Neural network systems can be used to compress first class dynamics, as shown in 2e. The absolute error is presented in 2f. Deep Neural networks with fractinal derivatives is a new machine learning techniques for the comprehensive solution of complex mathematical and physiscal problems.

Representation of class $I_c(t)$ graphically, we focused on the dynamics of said class with the help of deep Neural network in Fig:3a. Here, we note that the approximate RC is 1, the ME is $9.6346e-10$ and RMS is $3.104e-05$. According to the histogram the applied method has a ME $2.8036e-07$ and varience error is $3.1038e-05$. Using the same procedure for the train data we have the graphs in 3b. The graph represents RC 1, the maen and RMS errors are $9.6393e-10$ and $3.1047e-05$ respectively. From the plot of histogram we see that the ME is $3.2634e-07$ and the varience error is $3.1046e-05$. In 3c, with the help of deep Neural network the test data is presented graphycall. The regression coefficinet is 1, ME and RMS error are $9.7347e-10$ and $3.12e-05$ respectively. In histogram, the ME and varience error $2.972e-07$ and $3.12e-05$ accordingly. In 3d we see that the validation regression analysis is 1, maen erroer and RMS error are $9.5128e-10$ and $3.0843e-05$. From the histigram we confirm that the ME is $4.8936e-08$ and the varience error is $3.0843e-05$. Additonally, fractional order and deep Neural network can be used to compress first class dynamics, as shown in 3e. The absolute error is presented in 3f. Deep Neural networks with fractinal derivatives is a new machine learning techniques for the comprehensive solution of complex mathematical and physiscal problems.

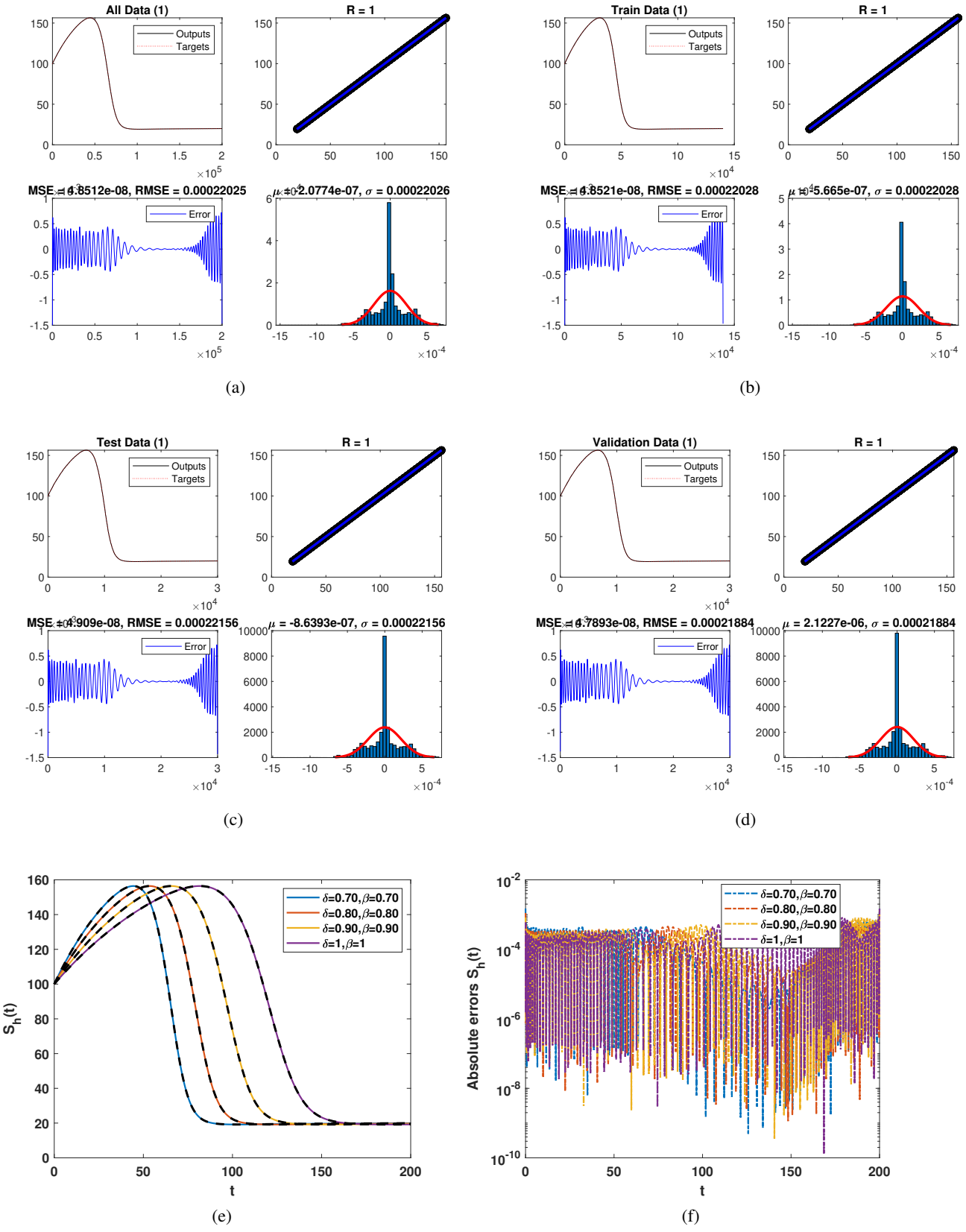

Fig. 1: Using deep Neural network, the dynamics of $S_h(t)$ (a) all data, (b) train data, (c) test data (d) validation, (e) comparison of FFC with NN, (f) integer order and non-integer orders comparison.

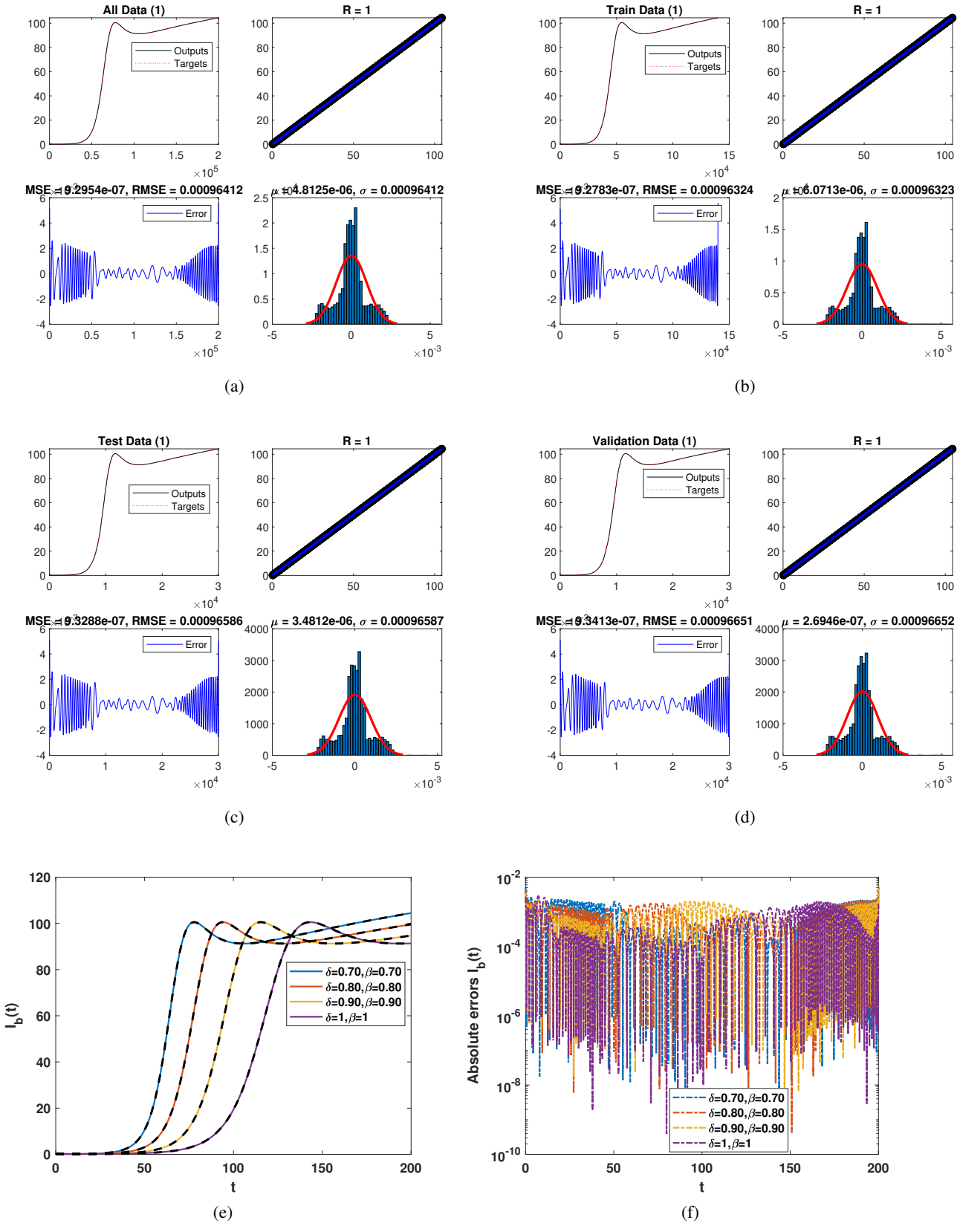

Fig. 2: Using deep Neural network, the dynamics of $I_b(t)$ (a) all data, (b) train data, (c) test data (d) validation, (e) comparison of FFC with NN, (f) integer order and non-integer orders comparison.

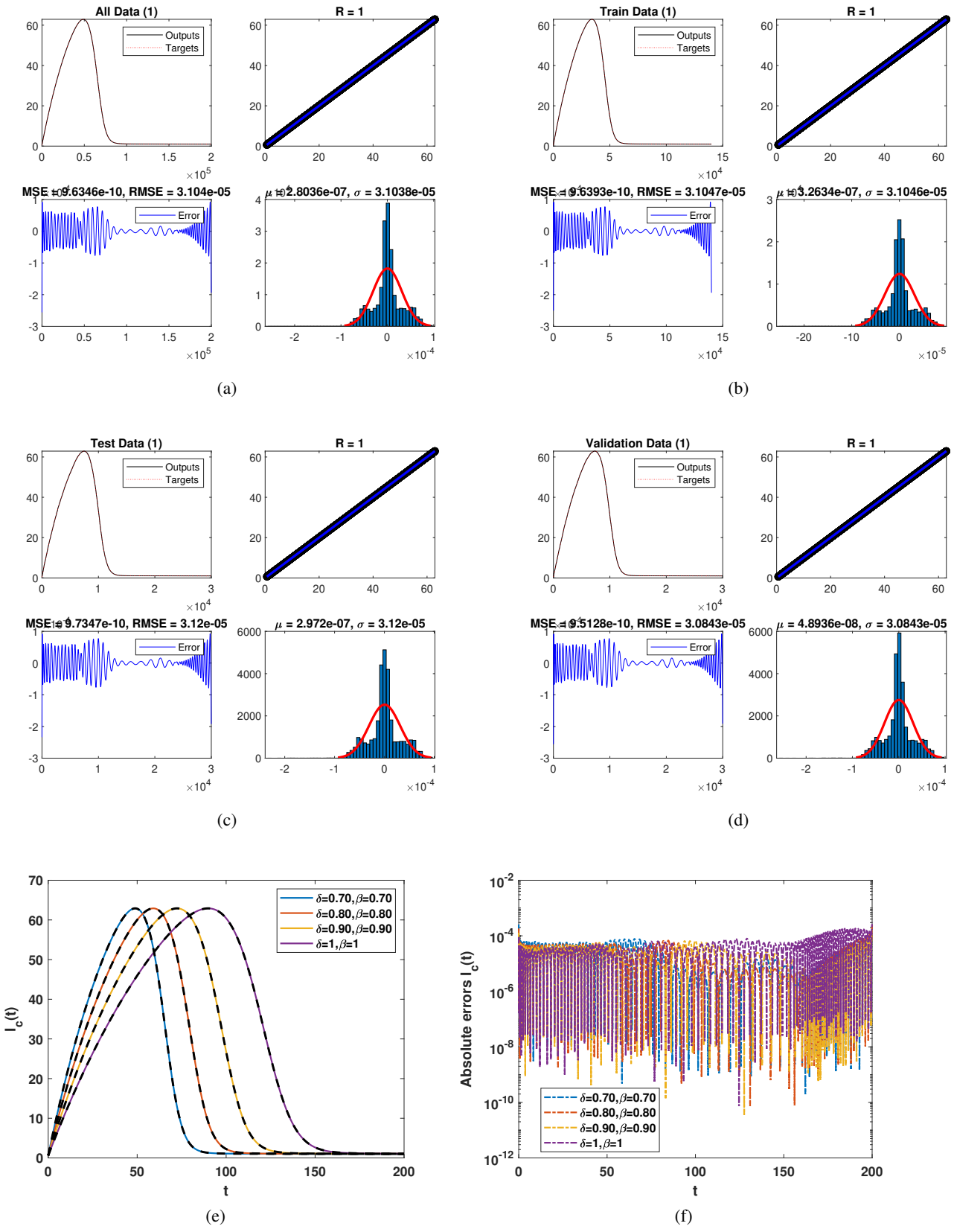

Fig. 3: Using deep Neural network, the dynamics of $I_c(t)$ (a) all data, (b) train data, (c) test data (d) validation, (e) comparison of FFC with NN, (f) integer order and non-integer orders comparison.

In the representation of class $D_{bc}(t)$, we observe the dynamics of the said class with the help of deep Neural network in Fig:4a. Here, we note that the approximate RC is 1, the ME is $5.6548e-09$ and RMS is $7.5199e-05$. According to the histogram the applied method has a ME $2.3573e-07$ and varience error is $7.5198e-05$. Using the same process for the train data we have the graphs in 4b, where the graph represents RC 1, the mean and RMS errors are $5.6564e-09$ and $7.5209e-05$ respectively. From the plot of histogram, we see that the ME is $2.0078e-07$ and the varience error is $7.5209e-05$. In 4c, with the aid of deep Neural network the test data is presented graphycall, where the regression coefficinet is 1, ME and RMS error are $5.6077e-09$ and $7.4884e-05$ respectively. In histogram, the ME is $-5.8581e-07$ and the varience errors is $7.4883e-05$. From 3d, we have validation regression analysis is 1, maen erroer $5.6947e-09$ and RMS error is $7.5463e-05$. The histigram confirmed that the ME is $-4.8767e-08$ and the varience error is $7.5465e-05$. Additonally, fractional order and deep Neural network can be used to compress first class dynamics, as shown in 4e. The absolute error is presented in 4f.

In the graphs of class $R_b(t)$, we note that the dynamics of the class with the help of deep Neural network in Fig:5a. Here, we have the approximate RC is 1, the ME is $7.7333e-09$ and RMS is $8.7939e-05$. According to the histogram the applied method has a ME $1.7168e-07$ and varience error is $8.7939e-05$. Using the same procedure for the train data we have the graphs in 5b, where the graph represents RC 1, the mean and RMS errors are $7.779e-09$ and $8.8199e-05$ respectively. In histogram, we see that the ME is $6.4213e-08$ and the varience error is $8.8199e-05$. In 5c, with the aid of deep Neural network the test data is presented graphycall, where the regression coefficinet is 1, ME is $7.8419e-09$ and RMS error is $8.8555e-05$. In histogram, the ME is $-9.0769e-09$ and the varience errors is $8.8556e-05$. From 5d, we have validation regression analysis is 1, maen erroer $7.4109e-09$ and RMS error is $8.6087e-05$. The histigram confirm that the ME is $8.5393e-07$ and the varience error is $8.6084e-05$. Moreover, fractional order and deep Neural network can be used to compress first class dynamics, as shown in 5e. The absolute error is presented in 5f.

In the graphical representation of class $R_c(t)$, we see that the dynamics of the class with the help of deep Neural network in Fig:6a. Here, the approximate RC is 1, the ME is $1.1993e-09$ and RMS is $3.4631e-05$. In histogram the ME $2.8401e-08$ and varience error is $3.4631e-05$. Similarly, the same procedure for the train data we have the graphs in 6b, where the graph represents RC 1, the mean and the RMS errors are $1.1977e-09$ and $3.4608e-05$ respectively. In histogram, we see that the ME is $-4.7557e-09$ and the varience error is $3.4608e-05$. In 6c, with the aid of deep Neural network the test data is presented graphycall, where the regression coefficinet is 1, ME is $1.1966e-09$ and RMS error is $3.4591e-05$. In histogram, the ME is $4.9834e-08$ and the varience errors is $3.4592e-05$. From 6d, we have validation regression analysis is 1, maen erroer $1.2095e-09$ and RMS error is $3.4777e-05$. The histigram confirm that the ME is $1.617e-07$ and the varience error is $3.4778e-05$. Moreover, fractional order and deep Neural network can be used to compress first class dynamics, as shown in 6e. The absolute error is presented in 6f.

The graphical representation of class $R_{bc}(t)$, we note that the dynamics of the class with the help of deep Neural network in Fig:7a. Here, the approximate RC is 1, the ME is $1.3351e-07$ and RMS is 0.00036539. In histogram the ME $-2.1405e-07$ and varience error is 0.0003654. Similarly, the same procedure for the train data we have the graphs in 7b, where the graph represents RC 1, the mean and the RMS errors are $1.3368e-07$ and 0.00036563 respectively. In histogram, we see that the ME is $1.8453e-07$ and the varience error is 0.00036563. In 7c, with the aid of deep Neural network the test data is presented graphycall, where the regression coefficinet is 1, ME is $1.3403e-07$ and RMS error is 0.0003661. In histogram, the ME is $-1.2481e-06$ and the varience errors is 0.00036611. From 7d, we have validation regression analysis is 1, maen erroer $1.3219e-07$ and RMS error is 0.00036358. The histigram confirm that the ME is $-1.04e-06$ and the varience error is 0.00036359. Moreover, fractional order and deep Neural network can be used to compress first class dynamics, as shown in 7e. The absolute error is presented in 7f.

The graphical representation of class $B(t)$, we note that the dynamics of the class with the help of deep Neural network in Fig:8a. Here, the approximate RC is 1, the ME is $1.6872e-07$ and RMS is 0.00041075. In histogram the ME $1.5299e-06$ and varience error is 0.00041075. Similarly, the same procedure for the train data we have the graphs in 8b, where the graph represents RC 1, the mean and the RMS errors are $1.7602e-07$ and 0.00041955 respectively. In histogram, we see that the ME is $1.3928e-06$ and the varience error is 0.00041955. In 8c, with the aid of deep Neural network the test data is presented graphycall, where the regression coefficinet is 1, ME is $1.4754e-07$ and RMS error is 0.00038411. In histogram, the ME is $-5.9377e-07$ and the varience errors is 0.00038411. From 8d, we have validation regression analysis is 1, maen erroer $1.558e-07$ and RMS error is 0.00039471. The histigram confirm that the ME is $4.2938e-06$ and the varience error is 0.0003947. Moreover, fractional order and deep Neural network can be used to compress first class dynamics, as shown in 8e. The absolute error is presented in 8f.

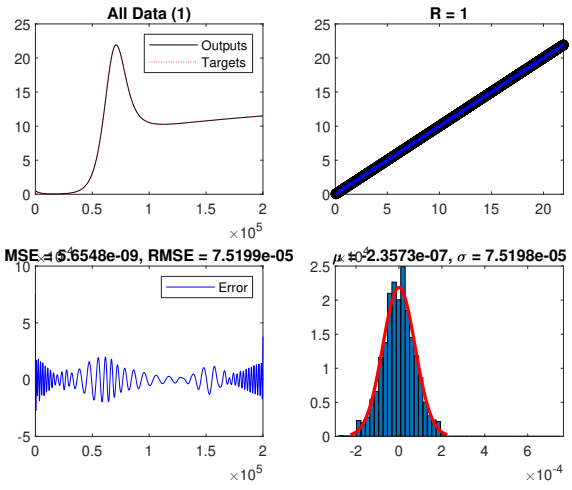

(a)

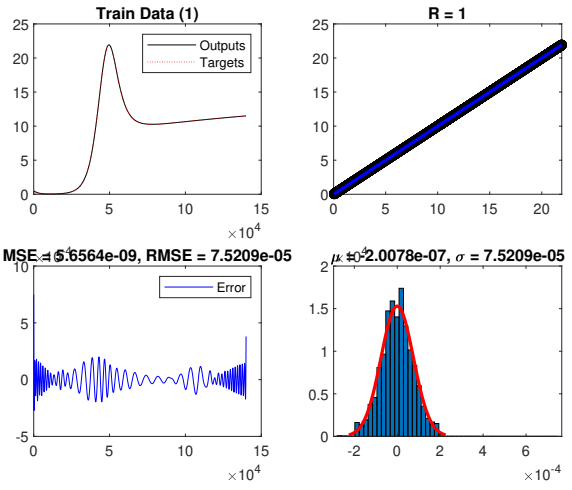

(b)

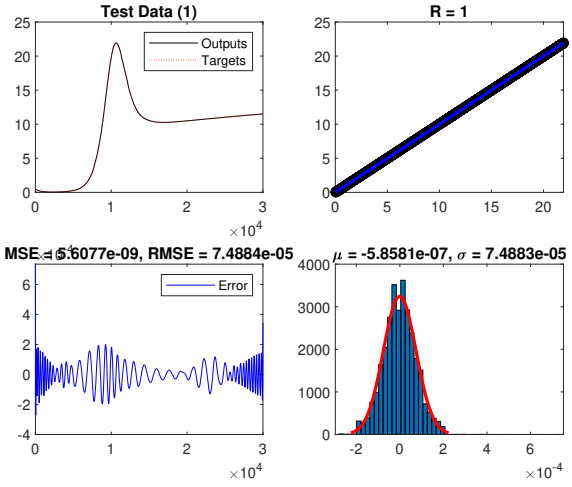

(c)

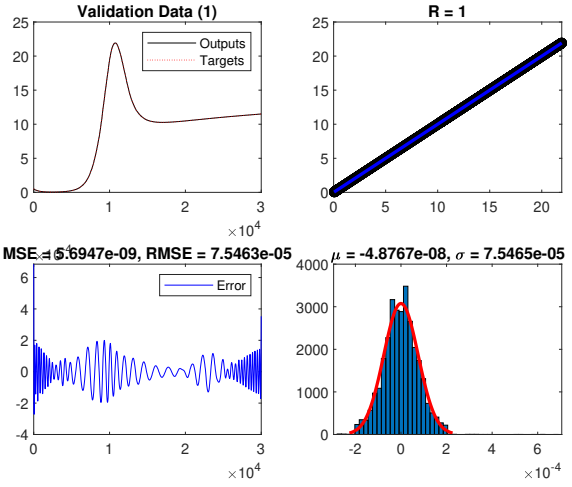

(d)

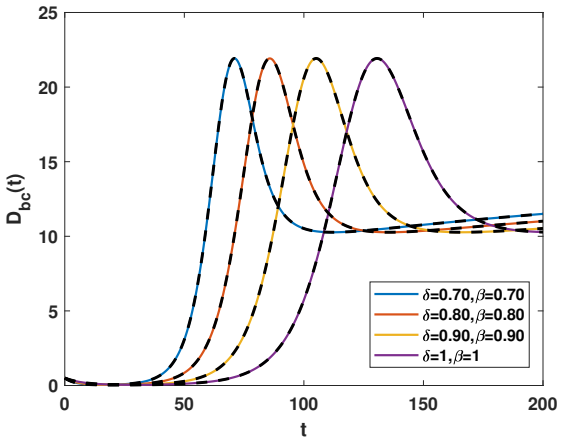

(e)

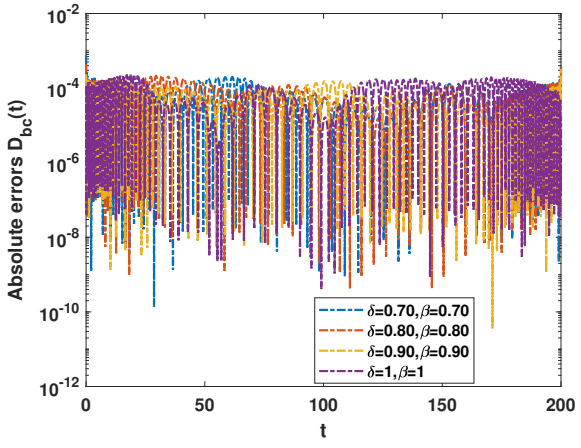

(f)

Fig. 4: Using deep Neural network, the dynamics of $D_{bc}(t)$ (a) all data, (b) train data, (c) test data (d) validation, (e) comparison of FFC with NN, (f) integer order and non-integer orders comparison.

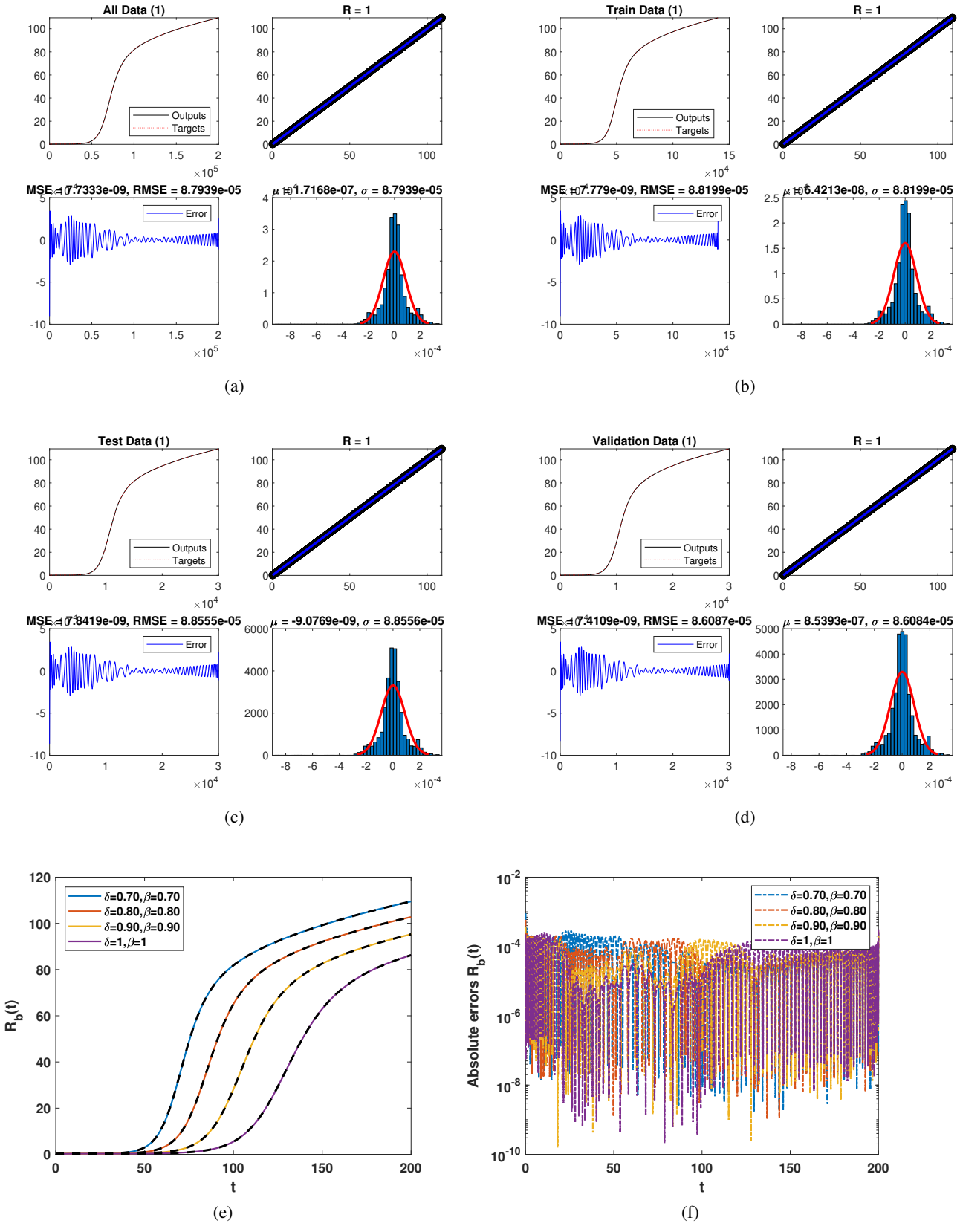

Fig. 5: Using deep Neural network, the dynamics of $R_b(t)$ (a) all data, (b) train data, (c) test data (d) validation, (e) comparison of FFC with NN, (f) integer order and non-integer orders comparison.

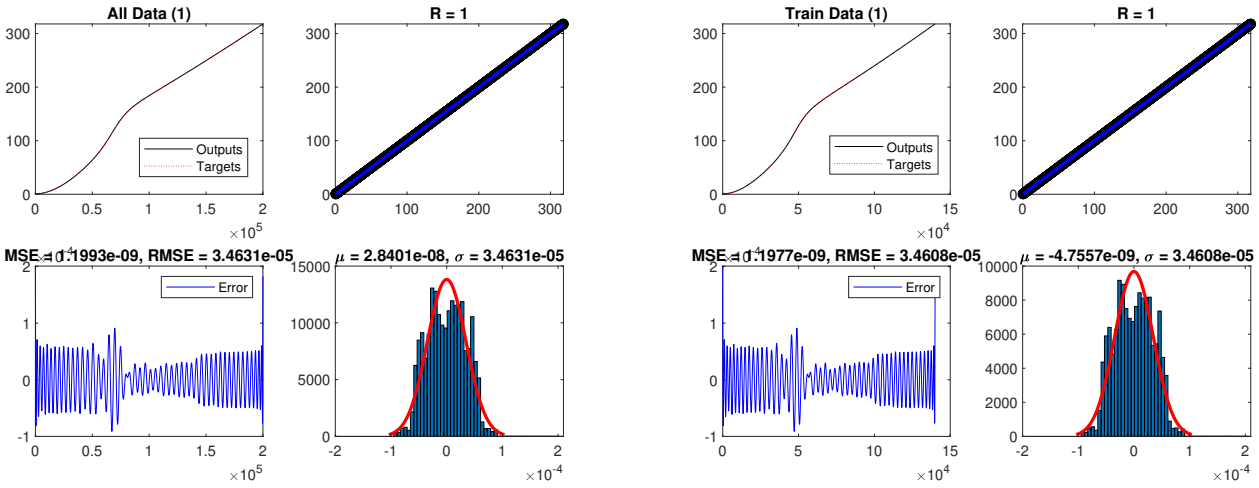

(a)

(b)

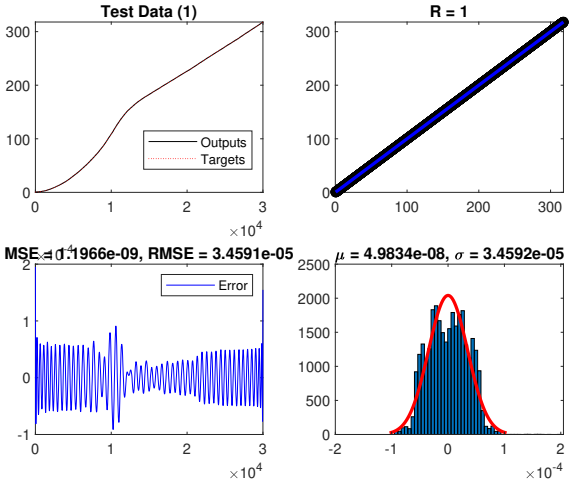

(c)

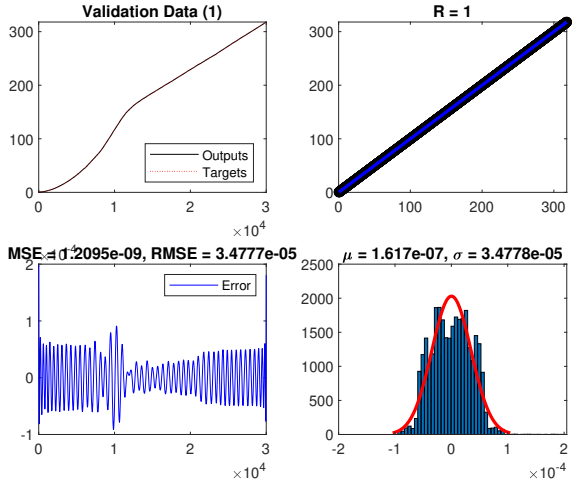

(d)

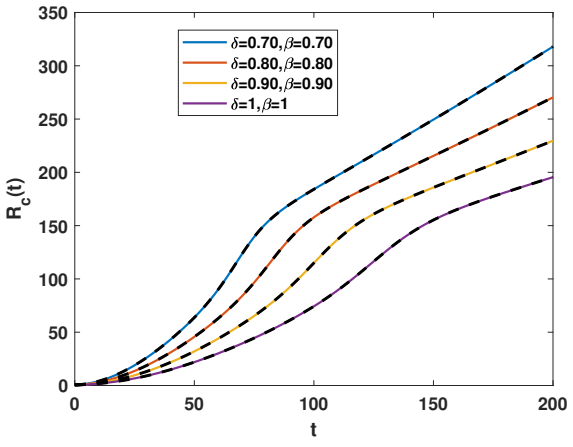

(e)

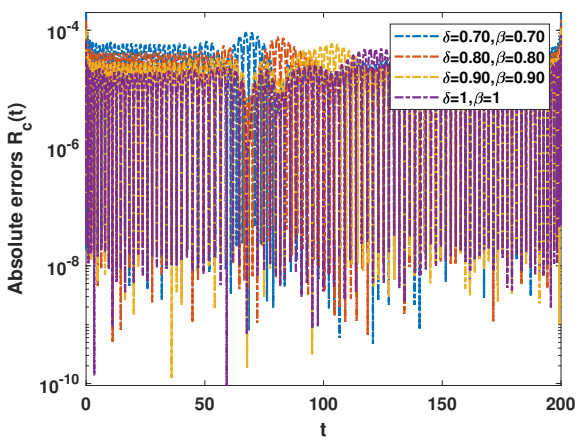

(f)

Fig. 6: Using deep Neural network, the dynamics of $R_c(t)$ (a) all data, (b) train data, (c) test data (d) validation, (e) comparison of FFC with NN, (f) integer order and non-integer orders comparison.

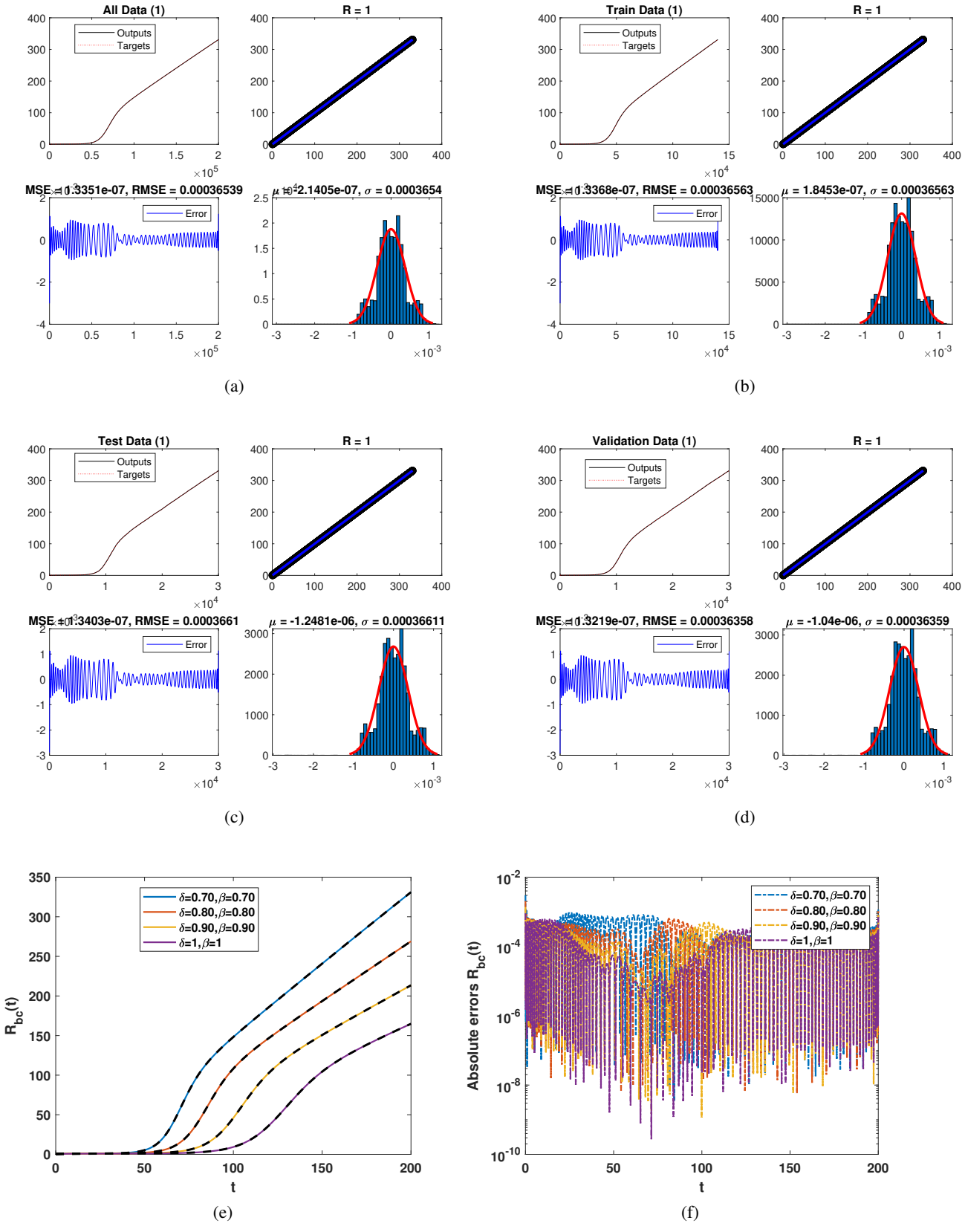

Fig. 7: Using deep Neural network, the dynamics of $R_{bc}(t)$ (a) all data, (b) train data, (c) test data (d) validation, (e) comparison of FFC with NN, (f) integer order and non-integer orders comparison.

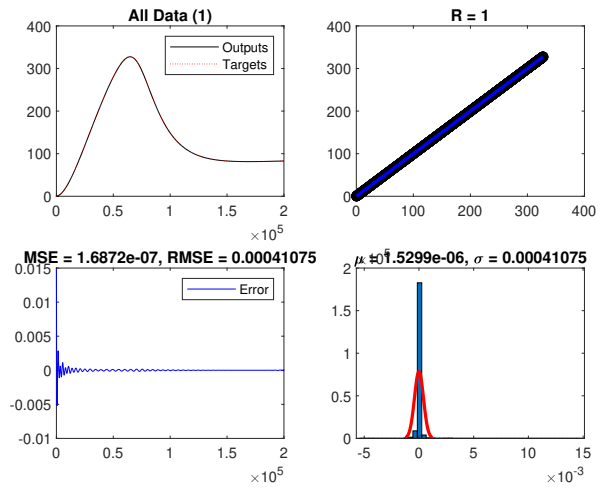

(a)

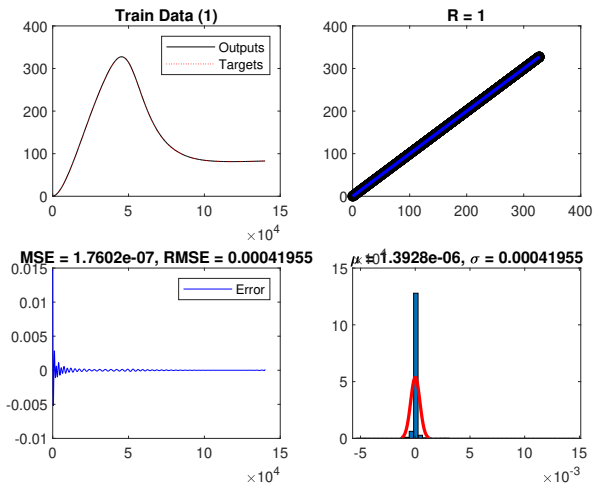

(b)

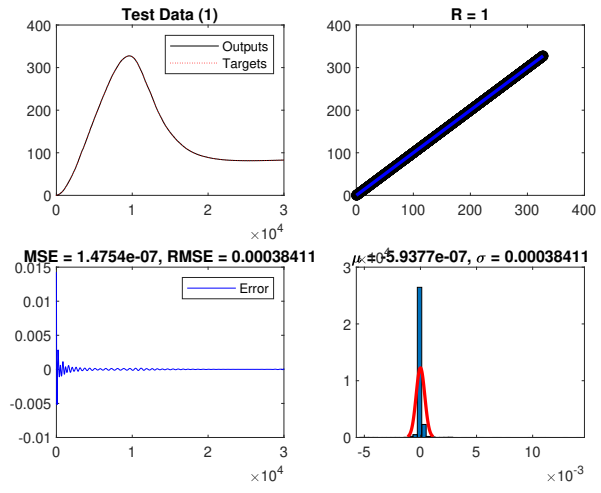

(c)

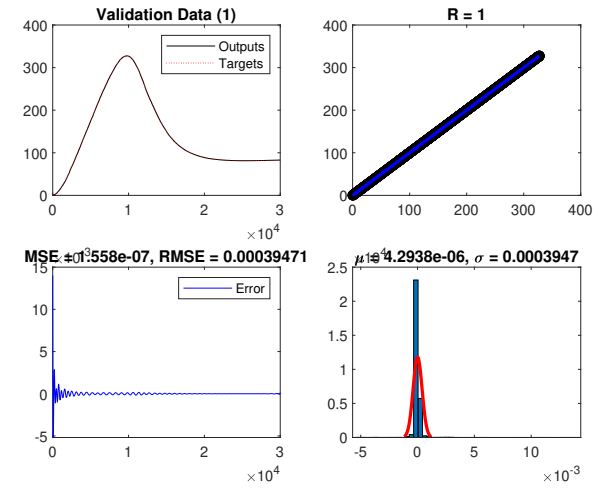

(d)

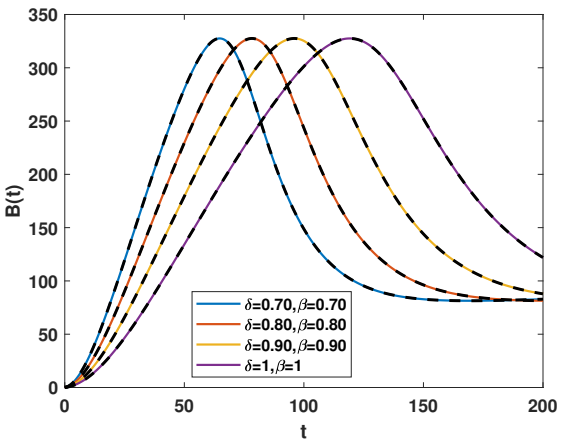

(e)

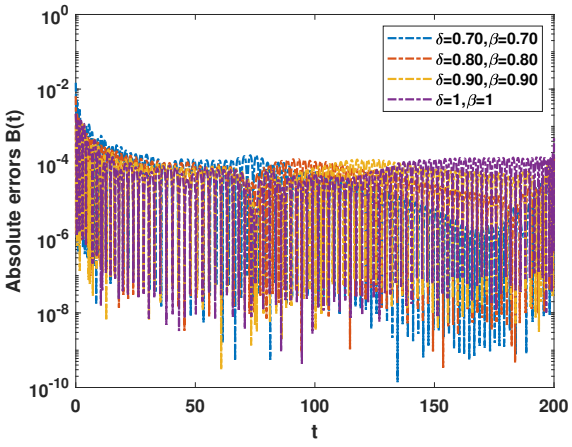

(f)

Fig. 8: Using deep Neural network, the dynamics of $B(t)$ (a) all data, (b) train data, (c) test data (d) validation, (e) comparison of FFC with NN, (f) integer order and non-integer orders comparison.

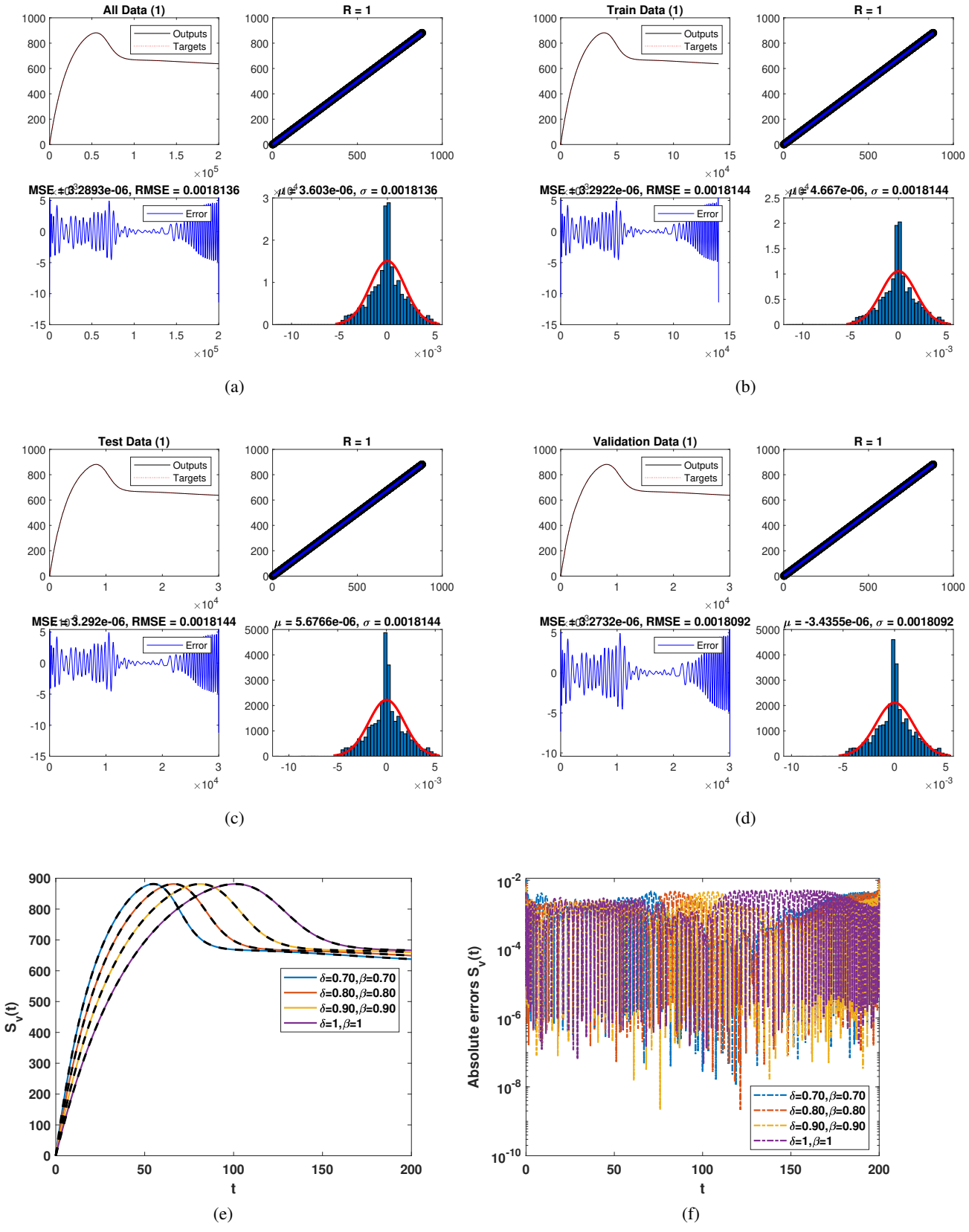

Fig. 9: Using deep Neural network, the dynamics of $S_v(t)$ (a) all data, (b) train data, (c) test data (d) validation, (e) comparison of FFC with NN, (f) integer order and non-integer orders comparison.

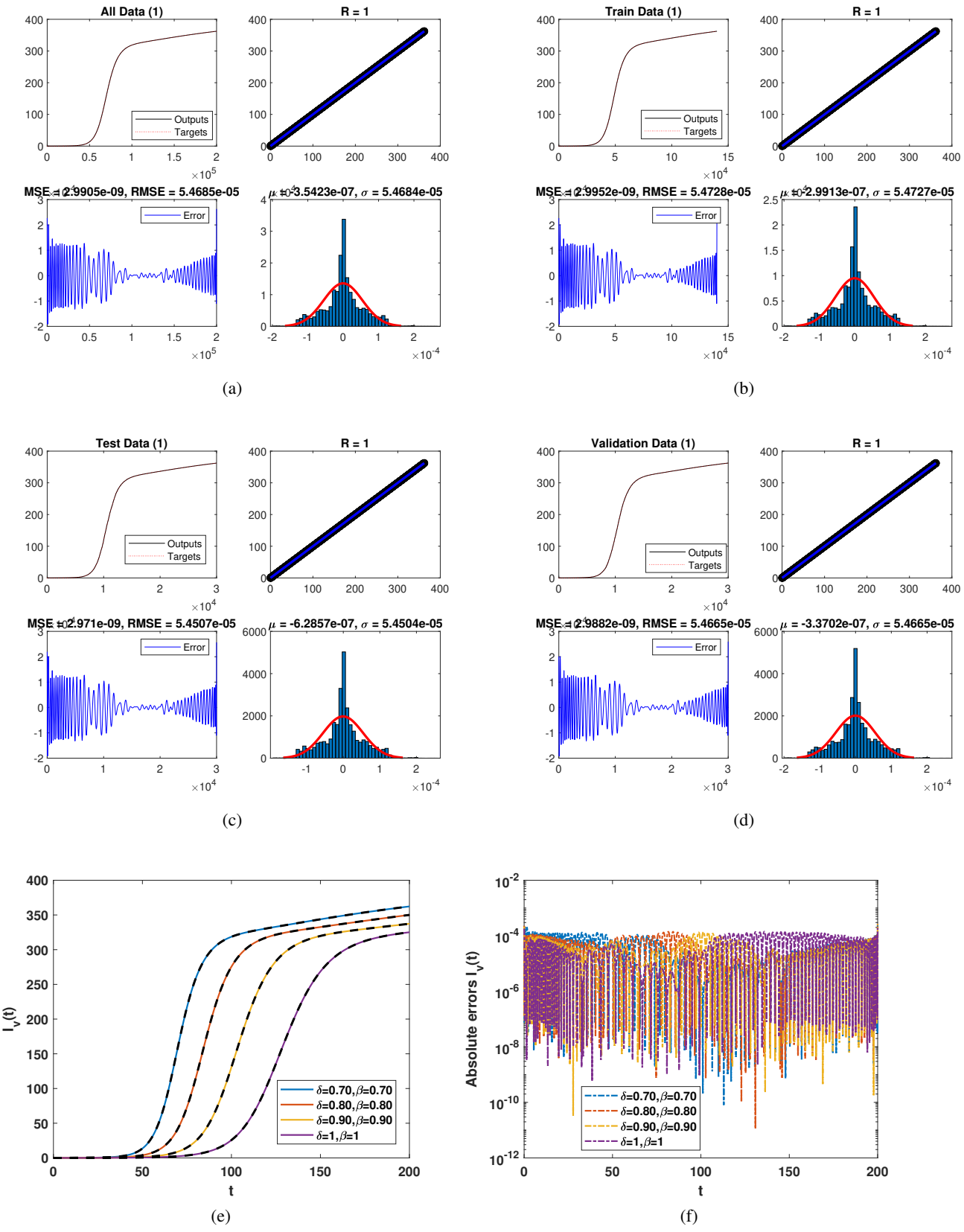

Fig. 10: Using deep Neural network, the dynamics of $I_v(t)$ (a) all data, (b) train data, (c) test data (d) validation, (e) comparison of FFC with NN, (f) integer order and non-integer orders comparison.

The graphical representation of class $S_v(t)$, we note that the dynamics of the class with the help of deep Neural network in Fig:9a. Here, the approximate RC is 1, the ME is $3.2893e-06$ and RMS is 0.0018136. In histogram the ME $3.603e-06$ and varience error is 0.0018136. Similarly, the same procedure for the train data we have the graphs in 9b, where the graph represents RC 1, the mean and the RMS errors are $3.2922e-06$ and 0.0018144 respectively. In histogram, we see that the ME is $4.667e-06$ and the varience error is 0.0018144. In 9c, with the aid of deep Neural network the test data is presented graphycall, where the regression coefficinet is 1, ME is $3.292e-06$ and RMS error is 0.0018144. In histogram, the ME is $5.6766e-06$ and the varience errors is 0.0018144. From 9d, we have validation regression analysis is 1, maen erroer $3.2732e-06$ and RMS error is 0.0018092. The histigram confirm that the ME is $-3.4355e-06$ and the varience error is 0.0018092. Moreover, fractional order and deep Neural network can be used to compress first class dynamics, as shown in 9e. The absolute error is presented in 9f.
The graphical representation of class $I_v(t)$, we note that the dynamics of the class with the help of deep Neural network in Fig:10a. Here, the approximate RC is 1, the ME is $2.9905e-09$ and RMS is $5.4685e-05$. In histogram the ME $3.5423e-07$ and varience error is $5.4684e-05$. Similarly, the same procedure for the train data we have the graphs in 10b, where the graph has RC 1, the mean and the RMS errors are $2.9952e-09$ and $5.4728e-05$ respectively. In histogram, we see that the ME is $2.9913e-07$ and the varience error is $5.4727e-05$. In 10c, with the aid of deep Neural network the test data is presented graphycall, where the regression coefficinet is 1, ME is $2.971e-09$ and RMS error is $5.4507e-05$. In histogram, the ME is $-6.2857e-07$ and the varience errors is $5.4504e-05$. From 10d, we have validation regression analysis is 1, maen erroer $2.9882e-09$ and RMS error is $5.4665e-05$. The histigram confirm that the ME is $-3.3702e-07$ and the varience error is $5.4665e-05$. Moreover, fractional order and deep Neural network can be used to compress first class dynamics, as shown in 10e. The absolute error is presented in 10f.

7 Conclusion

In this study, we use a fractional order mathematical model to thoroughly examine the dynamics of cholera and Buruli ulcer. Using evolutionary differential equations, the model for the co-dynamics buruli Ulcer and cholera infections as well as their dual infection are successfully created. The proposed model is investigated and the desired results were obtained and discussed. The effects of BU on cholera and vice versa are examined, and useful information is recommended. The comprehensive study of the dynamics of a Buruli ulcer and cholera model on fractal-fractional Caputo derivative is the main task in this paper. After the basic definitions we apply theorem of functional anlysis to investigate the qualitatitve analysis for the proposed model. The fractional-order problems are also numerically approximated using iterative methods, facilitating the exploration of dynamics within the nanotechnology domain through a systematic approach. This method effectively explores continuous spectrum dynamics ranging from 0 to 1, moving beyond merely focusing on discrete dynamics. For various non-integer orders κ and fractional dimensions τ, the Adams Bashforth numerical scheme is applied for dynamical behaviuor of each compartment. The graphical behaviour of each class density lies in between two integers. Low non-integer orders and fractal dimensions need short memory interval for stability and convergence. Deep neural network, a navel approach is applied to the model analysis havin two hidden layers with 50 and 5 neurons initially. The model's dataset, comprising two distenct fractional order within category is partitioned into three subset. This structure facilitate the plotting and examination of each class's dynamics, as well as the evaluation of the corresponding absolute error. The comparison between integer and fractional orders confirms that classical models may underestimate persistence effects in co-infection dynamics, whereas the proposed fractal–fractional framework provides a more realistic description of long-term disease behavior.

Declarations

Conflict of interest

The authors declare that they have no conflict of interest.

Data availability

No data was used or generated in the paper.

Authorship contribution statement

The authors have equally contributed to the paper. All authors read and approved the final manuscript.

Acknowledgment

The authors extend their appreciation to Prince Sattam bin Abdulaziz University for funding this research work through the project number (PSAU/2025/03/34359).

References

[1] M. A. Khan, Z. Hammouch, D. Baleanu, Modeling the dynamics of hepatitis E via the Caputo-Fabrizio derivative, *Mathematical Modelling of Natural Phenomena*, **14(3)**, (2019), 311.

[2] K. M. Owolabi, Z Hammouch, Mathematical modeling and analysis of two-variable system with noninteger-order derivative, *Chaos: An Interdisciplinary Journal of Nonlinear Science*, **29(1)**, (2019).
[3] J. Singh, K. Devendra, Z. Hammouch, A. Atangana, A fractional epidemiological model for computer viruses pertaining to a new fractional derivative, *Applied mathematics and computation*, **316** (2018), 504-515.
[4] A. Atangana, S. I. Araz, New concept in calculus Piecewise differential and integral operators, *Chaos, Solitons & Fractals* **145**, (2021), 110638.
[5] A. Atangana, S. I. Araz, Modeling third waves of Covid-19 spread with piecewise differential and integral operators Turkey, Spain, and Czechia, *Results in Physics*, **29**, (2021), 104694.
[6] N. J. White, C. Faust, Manson's tropical infectious diseases, Chapter (43), Malaria, *Elsevier*, Editor (2014).
[7] WHO, March. Global health observatory data repository, *World Health Organization* (2015).
[8] K. Asiedu, S. Etuaful, Socioeconomic implications of Buruli ulcer in Ghana a three-year review, *The American journal of tropical medicine and hygiene*, **59(6)**, (1998), 1015-1022.
[9] S. Etuaful, B. Carbonnelle, J. Grosset, S. Lucas, C. Horsfield, R. Phillips, M. Evans et al., Efficacy of the combination rifampin-streptomycin in preventing growth of Mycobacterium ulcerans in early lesions of Buruli ulcer in humans, *Antimicrobial agents and chemotherapy*, **49(8)**, (2005), 3182-3186.
[10] A. Chauty, M. F. Ardant, A. Adeye, H. Euverte, A. Guédeénon, C. Johnson, J. Aubry, E. Nuermberger, J. Grosset, Promising clinical efficacy of streptomycin-rifampin combination for treatment of buruli ulcer (Mycobacterium ulcerans disease), *Antimicrobial agents and chemotherapy*, **51(11)**, (2007), 4029-4035.
[11] W. A. Nienhuis, Y. Stienstra, W. A. Thompson, P. C. Awuah, K. M. Abass, W. Tuah, N. Y. Awua-Boateng et al., Antimicrobial treatment for early, limited Mycobacterium ulcerans infection: a randomised controlled trial, *The Lancet*, **375(9715)**, (2010), 664-672.
[12] K. P. Grietens, Koen, A. U. Boock, H. Peeters, S. H. Muela, E. Toomer, J. M. Ribera, Ït is me who endures but my family that suffers¨ social isolation as a consequence of the household cost burden of Buruli ulcer free of charge hospital treatment, *PLoS Neglected Tropical Diseases*, **2(10)**, (2008), e321.
[13] K. Asiedu, S. Etuaful, Socioeconomic implications of Buruli ulcer in Ghana a three-year review, *The American journal of tropical medicine and hygiene*, **59(6)**, (1998), 1015-1022.
[14] A. Y. Aidoo, B. Osei, Prevalence of aquatic insects and arsenic concentration determine the geographical distribution of Mycobacterium ulcerans infection, *Computational and Mathematical Methods in Medicine*, **8(4)**, (2007), 235-244.
[15] D. Ofori-Adjei, K. Koram, Of cholera and Ebola virus disease in Ghana, *Ghana medical journal*, **48(3)**, (2014), 120.
[16] J. O. M. Pobee, F. Grant, Case report of cholera, *Ghana Med J*, **9(4)**, (1970), 306-9.
[17] Record, Weekly Epidemiological, Cholera vaccines WHO position paper, *WEEKLY EPIDEMIOLOGICAL RECORD* **26(13)**, (2010).
[18] B. F. Osei, A. A. Duker, E. Augustijn, A. Stein, Spatial dependency of cholera prevalence on potential cholera reservoirs in an urban area, Kumasi, Ghana, *International Journal of Applied Earth Observation and Geoinformation*, **12(5)**, (2010), 331-339.
[19] D. Ruiz-Moreno, M. Pascual, M. Emch, M. Yunus, Spatial clustering in the spatio-temporal dynamics of endemic cholera, *BMC infectious diseases*, **10**, (2010) 1-12.
[20] C. T. Codeço, Endemic and epidemic dynamics of cholera the role of the aquatic reservoir, *BMC Infectious diseases*, **1**, (2001), 1-14.
[21] D. M. Hartley, J. G. Morris Jr, D. L. Smith, Hyperinfectivity a critical element in the ability of V. cholerae to cause epidemics?., *PLoS medicine* **3(1)**, (2006), e7.
[22] Z. Mukandavire, S. Liao, J. Wang, H. Gaff, D. L. Smith, J. Glenn Morris Jr, Estimating the reproductive numbers for the 2008–2009 cholera outbreaks in Zimbabwe, *Proceedings of the National Academy of Sciences*, **108(21)**, (2011), 8767-8772.
[23] R. L. M. Neilan, E. Schaefer, H. Gaff, K. R. Fister, S. Lenhart, Modeling optimal intervention strategies for cholera, *Bulletin of mathematical biology*, **72**, (2010), 2004-2018.
[24] K. O. Okosun, O. D. Makinde, A co-infection model of malaria and cholera diseases with optimal control, *Mathematical biosciences*, **258**, (2014), 19-32.
[25] E. Bonyah, I. Dontwi, F. Nyabadza, A theoretical model for the transmission dynamics of the Buruli ulcer with saturated treatment, *Computational and Mathematical Methods in Medicine*, **2014(1)**, (2014), 576039.
[26] F. Nyabadza, E. Bonyah, On the transmission dynamics of Buruli ulcer in Ghana Insights through a mathematical model, *BMC research notes*, **8**, (2015), 1-15.
[27] Podlubny, Igor. Fractional differential equations: an introduction to fractional derivatives, fractional differential equations, to methods of their solution and some of their applications. Vol. 198. elsevier, 1998.
[28] Metzler, Ralf, and Joseph Klafter. "The restaurant at the end of the random walk: recent developments in the description of anomalous transport by fractional dynamics." Journal of Physics A: Mathematical and General 37, no. 31 (2004): R161.
[29] Mainardi, Francesco. Fractional calculus and waves in linear viscoelasticity: an introduction to mathematical models. World Scientific, 2022.
[30] Atangana, Abdon, and Dumitru Baleanu. "New fractional derivatives with nonlocal and non-singular kernel: theory and application to heat transfer model." arXiv preprint arXiv:1602.03408 (2016).
[31] Haidong, Qu, Mati Ur Rahman, and Muhammad Arfan. "Fractional model of smoking with relapse and harmonic mean type incidence rate under Caputo operator." Journal of Applied Mathematics and Computing 69, no. 1 (2023): 403-420.

[32] Liu, Xuan, Mati ur Rahmamn, Saeed Ahmad, Dumitru Baleanu, and Yasir Nadeem Anjam. "A new fractional infectious disease model under the non-singular Mittag–Leffler derivative." Waves in Random and Complex Media 35, no. 1 (2025): 1617-1643.
[33] Saleem, Ayesha, Mati ur Rahman, Salah Boulaaras, Rafik Guefaifia, and Dumitru Baleanu. "Exploring the dynamics of HIV and HCV co-infection through piecewise modified Mittag-Leffler fractional derivatives." Applied Mathematics in Science and Engineering 33, no. 1 (2025): 2478038.
[34] Chen, Wen, Hongguang Sun, Xiaodi Zhang, and Dean Korošak. "Anomalous diffusion modeling by fractal and fractional derivatives." Computers & Mathematics with Applications 59, no. 5 (2010): 1754-1758.
[35] Li, Zhongfei, Zhuang Liu, and Muhammad Altaf Khan. "Fractional investigation of bank data with fractal-fractional Caputo derivative." Chaos, Solitons & Fractals 131 (2020): 109528.
[36] Liu, Xuan, Shabir Ahmad, Mati ur Rahman, Yasir Nadeem, and Ali Akgül. "Analysis of a TB and HIV co-infection model under Mittag-Leffler fractal-fractional derivative." Physica Scripta 97, no. 5 (2022): 054011.
[37] ur Rahman, Mati. "Generalized fractal–fractional order problems under non-singular Mittag-Leffler kernel." Results in Physics 35 (2022): 105346.
[38] Zhao, Jin-Qiang, Ebenezer Bonyah, Bing Yan, Muhammad Altaf Khan, K. O. Okosun, Mohammad Y. Alshahrani, and Taseer Muhammad. "A mathematical model for the coinfection of buruli ulcer and cholera." Results in Physics 29 (2021): 104746.
[39] E. Bonyah, I. Dontwi, F. Nyabadza, Optimal Control Applied to the Spread of Buruli Uclcer, *American Journal of Computational and Applied Mathematics*, **4(3)**, (2014), 61-76.
[40] E. Bonyah, I. Dontwi, F. Nyabadza, An age-structured model for the spread of Buruli Ulcer Analysis and simulation in Ghana, *British Journal of Mathematics & Computer Science*, **4(16)**, (2014), 2298.
[41] A. Atangana, Fractal-fractional differentiation and integration: connecting fractal calculus and fractional calculus to predict complex system, *Chaos, solitons and fractals*, **102**, (2017), 396–406.
[42] A. Granas, J. Dugundji, "Fixed Point Theory", *Springer New York*, (2005).
[43] A. Atangana, Fractal-fractional differentiation and integration: connecting fractal calculus and fractional calculus to predict complex system, *Chaos, solitons & fractals*, **102**, (2017), 396-406.